

# Electronic and magnetic properties of SrTiO<sub>3</sub>/LaAlO<sub>3</sub> interfaces from first principles

Hanghui Chen<sup>1,3</sup>, Alexie M. Kolpak<sup>2,3</sup> and Sohrab Ismail-Beigi<sup>1,2,3</sup>

<sup>1</sup> *Department of Physics, Yale University, New Haven, CT 06570, USA*

<sup>2</sup> *Department of Applied Physics, Yale University, New Haven, CT 06570-8284, USA*

<sup>3</sup> *Center for Research on Interface Structures and Phenomena (CRISP),  
Yale University, New Haven, CT 06570-8284, USA*

(Dated: October 22, 2018)

## Abstract

A number of intriguing properties emerge upon the formation of the epitaxial interface between the insulating oxides LaAlO<sub>3</sub> and SrTiO<sub>3</sub>. These properties, which include a quasi two-dimensional conducting electron gas, low temperature superconductivity, and magnetism, are not present in the bulk materials, generating a great deal of interest in the fundamental physics of their origins. While it is generally accepted that the novel behavior arises as a result of a combination of electronic and atomic reconstructions and growth-induced defects, the complex interplay between these effects remains unclear. In this report, we review the progress that has been made towards unraveling the complete picture of the SrTiO<sub>3</sub>/LaAlO<sub>3</sub> interface, focusing primarily on present *ab initio* theoretical work and its relation to the experimental data. In the process, we highlight some key unresolved issues and discuss how they might be addressed by future experimental and theoretical studies.

## I. INTRODUCTION

With the advance of techniques to control thin film growth on the atomic scale, the study of epitaxial oxide heterostructures is a rapidly developing area of materials science [1–3]. Due to the ability to produce a well-defined, single-terminated surface [4, 5], oxide interfaces that are nearly atomically sharp can now be fabricated. In many cases, the properties of these interfaces turn out to be much richer than those of their bulk constituents [6–11]. Not only are these new interface phases of fundamental physical interest, they are also promising candidates for novel devices and technology.

One of the most interesting epitaxial oxide heterostructures to date is the (001) interface between  $\text{LaAlO}_3$  (LAO) and  $\text{SrTiO}_3$  (STO) [7]. Although both materials are conventional band insulators in bulk form, among the intriguing phenomena observed at the  $\text{SrTiO}_3/\text{LaAlO}_3$  interface is the presence of a high-mobility quasi two-dimensional electron gas [7, 12], which emerges when the  $\text{LaAlO}_3$  film thickness reaches a critical value of 1.6 nm (4  $\text{LaAlO}_3$  unit cells) [13, 14]. This thickness dependence enables external control of the conductivity of the heterostructure. Reversible control of the metal-insulator transition has been demonstrated via an applied electric field [13, 15]. In addition to these phenomena, at low temperature ( $\simeq 200$  mK), the  $\text{SrTiO}_3/\text{LaAlO}_3$  interface becomes superconducting [16–18]. Furthermore, though bulk  $\text{SrTiO}_3$  and  $\text{LaAlO}_3$  are both nonmagnetic, experiments suggest that the interface may exhibit some type of magnetic ordering [19]. In addition to fundamental scientific interests, the  $\text{LaAlO}_3/\text{SrTiO}_3$  interface is also promising for the development of novel applications in nanoscale oxide electronics. For example, devices have recently been fabricated [20] that exploit the fact that the interface conductivity can be “written” and “erased” locally with the aid of an atomic force microscope (AFM) tip [21, 22].

Despite extensive efforts in both theory [23–37] and experiment [38–47], the origins of these interface properties are not yet completely resolved. In part, this is due to the fact that more than one mechanism may play a role in determining the interesting behaviors. Also, which mechanism dominates the behavior in a given sample appears to be sensitive to the conditions under which the sample is grown and/or how it is processed prior to the experimental measurements [48]. As a result, direct comparison between experiments can be complicated. Nevertheless, progress is being made towards understanding the basis of the novel interface phenomena, in particular, the origin of the conductivity.

To date, three mechanisms have been proposed to account for the emergence of conductivity at the SrTiO<sub>3</sub>/LaAlO<sub>3</sub> interface. The first mechanism is an intrinsic electronic reconstruction due to the polar discontinuity at the interface [7, 12]. The driving force behind this mechanism can be understood in the following simple picture. Perovskite oxides have a generic  $ABO_3$  structure, where  $A$  and  $B$  are metal cations. Along the (001) direction, this structure consists of alternating  $AO$  and  $BO_2$  planes. In the simple ionic limit, SrTiO<sub>3</sub> consists of charge neutral layers, (SrO)<sup>0</sup> and (TiO<sub>2</sub>)<sup>0</sup>, while LaAlO<sub>3</sub> is composed of alternating charged layers, (LaO)<sup>+</sup> and (AlO<sub>2</sub>)<sup>-</sup>. The deposition of stoichiometric LaAlO<sub>3</sub> onto the SrTiO<sub>3</sub> (001) substrate is thus equivalent to the formation of a chain of capacitors in series. The potential across each capacitor is additive and, mathematically, diverges with the number of capacitors (*i.e.*, the thickness of the LaAlO<sub>3</sub> film). To offset the diverging potential, an electronic reconstruction, known as the “polar catastrophe”, is expected to occur, whereby half an electron (hole) is transferred to the  $n$ -type TiO<sub>2</sub>/LaO ( $p$ -type SrO/AlO<sub>2</sub>) interface so that the internal electric field through the LaAlO<sub>3</sub> film is completely compensated. As a consequence of this charge transfer, the interface becomes doped, leading to the observed conductivity.

The polar catastrophe mechanism is believed to be applicable to the SrTiO<sub>3</sub>/LaAlO<sub>3</sub> interface because of the multivalent nature of the Ti cations, which can exist as either Ti<sup>3+</sup> or Ti<sup>4+</sup>. Therefore, it is possible that this type of electronic reconstruction has a lower energy barrier and/or ground state energy than the typical atomic reconstructions that occur for more traditional semiconductor polar/non-polar interfaces [49, 50].

However, soon after the polar catastrophe mechanism was proposed, several groups [40–42] observed that the electronic properties of the interface are significantly affected by the presence of oxygen vacancies, a significant number of which are generated in the SrTiO<sub>3</sub> substrate during the LaAlO<sub>3</sub> deposition. These results suggest that oxygen vacancies can be responsible for the high sheet carrier densities and mobilities measured in experiments. Oxygen vacancies are also proposed [21] to account for the observed insulating-to-metallic transition, via a mechanism involving the creation and annihilation of oxygen vacancies on the LaAlO<sub>3</sub> surface. While the concentration of oxygen vacancies is suppressed by performing the LaAlO<sub>3</sub> film deposition under high oxygen partial pressures and/or post-annealing in oxygen, some residual conductance is still observed [13, 42], suggesting that oxygen vacancies may not be the sole source of the interface electron gas.

A third possible mechanism, based on the observed intermixing of cations across the SrTiO<sub>3</sub>/LaAlO<sub>3</sub> interface, has also been suggested [12, 38]. The driving force for cation mixing is assumed to be the reduction of the dipole energy at the interface. As such mixing results in the formation of La<sub>1-x</sub>Sr<sub>x</sub>TiO<sub>3</sub> [38], which is metallic when  $0.05 < x < 0.95$  [51, 52], it could also lead to interface conductivity.

Though each of the three mechanisms can explain particular experimental results, there is as yet no unified picture to describe the entire phase diagram of the SrTiO<sub>3</sub>/LaAlO<sub>3</sub> interface and the relations among the different phases. It is not clear whether the whole phase diagram has yet been identified, or whether some or all of these three mechanisms are adequate to account for the experimental observations.

The primary goals of this report are to review the progress made towards understanding the SrTiO<sub>3</sub>/LaAlO<sub>3</sub> interface using theoretical first principles calculations and to provide a theoretical perspective on the existing experimental data. We start by reviewing the experimental data in Section II, highlighting different results in the spirit of stimulating further studies. Section III reviews the state-of-the-art first-principles calculations on the SrTiO<sub>3</sub>/LaAlO<sub>3</sub> interface and discusses their successes and failures in describing the experimental observations. In Section IV, we pose what we think are the important unanswered questions about the SrTiO<sub>3</sub>/LaAlO<sub>3</sub> interface and in many cases try to suggest additional experiments and/or theoretical computations. Our conclusions are in Section V. The investigation of SrTiO<sub>3</sub>/LaAlO<sub>3</sub> interfaces is a rapidly growing field. Due to space limitations and the rapid publication of new results, we apologize to those whose work is not included here.

## II. EXPERIMENT

For (001) oriented growth of perovskites, two types of SrTiO<sub>3</sub>/LaAlO<sub>3</sub> interfaces are possible, depending on the sequence arrangement. The first has the atomic planes TiO<sub>2</sub>/LaO at the interface and is referred to as the *n*-type interface; the second is formed by adjacent SrO/AlO<sub>2</sub> planes and is called the *p*-type interface. Experimentally, it is the *n*-type interface that shows the interesting and novel properties mentioned in the introduction, while the *p*-type interface is found to be insulating. Below, we briefly review the experimental results on the *n*-type and *p*-type interfaces. For a more complete experimental review, especially

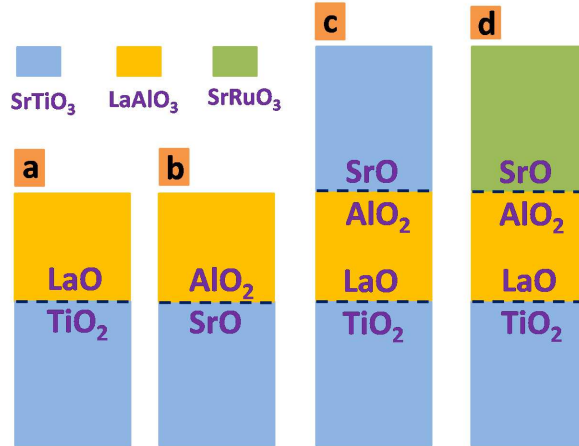


FIG. 1: Schematics of various types of SrTiO<sub>3</sub>/LaAlO<sub>3</sub> interfaces. The light blue denotes SrTiO<sub>3</sub>, the orange denotes LaAlO<sub>3</sub>, and the light green denotes SrRuO<sub>3</sub>. **a**) A bare *n*-type interface (TiO<sub>2</sub>/LaO) with AlO<sub>2</sub> terminated surface. **b**) A bare *p*-type interface (SrO/AlO<sub>2</sub>) with LaO terminated surface. **c**) An *np*-type interface with SrTiO<sub>3</sub> as the capping layer. **d**) A buried *n*-type interface with SrRuO<sub>3</sub> as the capping layer.

concerning the technical details, please refer to Refs. [53, 54].

### A. The *n*-type interface

The simplest *n*-type interface (which we call the “bare *n*-type interface”) has a TiO<sub>2</sub>-terminated SrTiO<sub>3</sub> substrate on which a LaAlO<sub>3</sub> film is grown, creating a TiO<sub>2</sub>/LaO interface and an exposed AlO<sub>2</sub>-terminated LaAlO<sub>3</sub> surface [7, 13] (see Fig. 1a). In addition, there are other variants. Huijben *et al.* [55] grew capping layers of SrTiO<sub>3</sub> on the LaAlO<sub>3</sub> to form a system with both *n*-type and *p*-type interfaces (*np*-type) (see Fig. 1c), while Wong *et al.* [56] grew SrRuO<sub>3</sub> electrodes as the capping layers on the LaAlO<sub>3</sub> to study the electric transport perpendicular to the interface (see Fig. 1d). These geometries create buried *n*-type interfaces. We briefly review and compare the experiments on these *n*-type interface systems.

#### 1. Transport

The transport properties of the *n*-type SrTiO<sub>3</sub>/LaAlO<sub>3</sub> interface depend on the oxygen partial pressure,  $p_{\text{O}_2}$ , at which the interface is grown, as well as whether and what type

of additional annealing steps are performed prior to transport measurements. The existing experimental measurements of the sheet resistance  $R_s$ , the sheet carrier density  $n_s$ , and the Hall mobility  $\mu_H$ , of samples grown at low oxygen partial pressure ( $\sim 10^{-6}$  mbar) without post-oxidization appear to have converged to the following values:  $R_s \sim 10^{-2} \Omega$ ,  $n_s \sim 10^{16} - 10^{17} \text{ cm}^{-2}$  and  $\mu_H \sim 10^4 \text{ cm}^2 \text{ V}^{-1}\text{s}^{-1}$  (see Table I).

Experiments measuring the transport properties of samples grown at low oxygen partial pressure ( $10^{-5} - 10^{-6}$  mbar) and then annealed in  $\text{O}_2$  reveal a range of results. Ohtomo *et al.* [7] do not find any significant change in the transport properties before and after annealing, whereas Kalabukhov *et al.* [40] grew samples under similar conditions, but observe an increase in  $R_s$  and decreases in  $n_s$  and  $\mu_H$  (see Table I) after annealing. Basletic *et al.* [57] find similar results to those observed by Kalabukhov *et al.* [40] for pre- and post-annealed samples.

There appears to be general agreement that, for samples grown at high oxygen partial pressures ( $\sim 10^{-4}$  mbar), the sheet carrier density is in the range  $10^{13} - 10^{14} \text{ cm}^{-2}$ . Some discrepancies arise in mobility measurements of the same type of samples: at low temperatures ( $\sim 5$  K),  $R_s \sim 10^4 \Omega$  and  $\mu_H \sim 10 \text{ cm}^2 \text{ V}^{-1}\text{s}^{-1}$  are obtained by Ohtomo *et al.* [7] and Herranz *et al.* [41], while Kalabukhov *et al.* [40] and Thiel *et al.* [16] report  $R_s$  and  $\mu_H$  values two orders of magnitude smaller and larger, respectively (see Table I).

It is noteworthy that the polar catastrophe mechanism [7, 12] predicts that 0.5 electrons per two-dimensional interface unit cell ( $0.5e/a_{\text{STO}}^2$ , where  $a_{\text{STO}}$  is the lattice constant of  $\text{SrTiO}_3$ ) at the  $n$ -type interface would completely cancel the internal electric field through the  $\text{LaAlO}_3$  film. That is equivalent to a sheet carrier density of  $3.3 \times 10^{14} \text{ cm}^{-2}$ , implying that the polar catastrophe should be the dominant mechanism determining the sheet carrier density in samples grown at high oxygen partial pressures ( $\sim 10^{-4}$  mbar), while other mechanisms, such as doping via oxygen vacancies, may be responsible for the higher sheet carrier densities of interfaces grown at lower oxygen partial pressures ( $\sim 10^{-6}$  mbar). However, agreement between the predicted and measured sheet carrier densities in samples grown at high oxygen partial pressure is not sufficient to rule out the possibility that other mechanisms, such as oxygen vacancies on the  $\text{LaAlO}_3$  surface [21], also play a role. These other possibilities may shed some light on the unexplained discrepancies in the measured mobilities in these samples.

We note that samples grown at very high oxygen partial pressures ( $> 10^{-2}$  mbar) [40] or

TABLE I: Values of sheet resistance  $R_s$ , sheet carrier density  $n_s$ , and Hall mobility  $\mu_H$  measured from transport in different studies. The data in this table are all taken at low temperature ( $T \sim 5$  K).

growth $p_{\text{O}_2}$ (mbar)	annealing conditions	$R_s(\Omega/\square)$	$n_s$ ( $\text{cm}^{-2}$ )	$\mu_H$ ( $\text{cm}^2 \text{V}^{-1}\text{s}^{-1}$ )	Ref.
$10^{-6}$	not annealed	$10^{-2}$	$10^{17}$	$10^4$	[7]
$10^{-6}$	annealed in 1 atm of $\text{O}_2$ at $400^\circ\text{C}$ for 2 hours	$10^{-2}$	$2 \times 10^{16}$	$10^4$	[7]
$10^{-6}$	not annealed	$10^{-2}$	$5 \times 10^{16}$	$10^4$	[40]
$10^{-6}$	annealed at 500 mbar during cooling	$10^3$	$10^{13}$	$10^3$	[40]
$10^{-6}$	annealed at 300 mbar during cooling	$10^2$	$3 \times 10^{13}$	$7 \times 10^2$	[57]
$10^{-6}$	not annealed	$3 \times 10^{-3}$		$10^4$	[41]
$10^{-6}$	not annealed		$2 \times 10^{16}$	$10^4$	[42]
$10^{-5}$	not annealed	$10^2$	$10^{16}$	$10^0$	[7]
$10^{-5}$	not annealed	$10^{-3}$	$5 \times 10^{17}$	$2 \times 10^3$	[57]
$2 \times 10^{-5}$	cooled at high oxidation		$2 \times 10^{13}$	$3 \times 10^2$	[42]
$10^{-4}$	not annealed	$10^4$	$10^{14}$	$10^1$	[7]
$10^{-4}$	not annealed	$10^2$	$10^{13}$	$10^3$	[40]
$10^{-4}$	annealed at 500 mbar during cooling	$10^2$	$10^{13}$	$10^3$	[40]
$10^{-4}$	not annealed	$3 \times 10^{-3}$		$10^1$	[41]
$5 \times 10^{-2}$	not annealed	insulating	insulating	insulating	[40]
$10^{-6} - 10^{-3}$	annealed at 300 mbar during cooling	insulating	insulating	insulating	[41]

samples annealed at high oxygen partial pressure [41] have been observed to be completely insulating. If post-annealing in oxygen fills oxygen vacancies and repairs the oxygen off-stoichiometry, then one would expect that with increasing oxygen partial pressure, the sheet

carrier density would asymptote to  $\sim 10^{14} \text{ cm}^{-2}$ , the value predicted for polar  $\text{LaAlO}_3$  and an ideal  $n$ -type interface as per the polar catastrophe mechanism. We will further discuss this situation in Section IV A.

Another factor affecting transport is the thickness of the  $\text{LaAlO}_3$  films. Samples grown under relatively high oxygen partial pressure ( $\sim 10^{-4}$  mbar) are not conducting unless the  $\text{LaAlO}_3$  film thickness exceeds a critical value, referred to as the “critical separation”. The two studies investigating the thickness dependence of sheet carrier density report critical separations of 4 and 6 unit cells [13, 42], respectively.

## 2. *Spatial extent and orbital character of the electron gas*

The oxygen partial pressure during the growth process affects not only the transport properties but also the spatial extent of the electron gas. Two different distributions of the electron gas have been observed. For samples grown at low oxygen partial pressure ( $\sim 10^{-6}$  mbar) and not subjected to further annealing, the electron gas extends over tens to hundreds of  $\mu\text{m}$  into the  $\text{SrTiO}_3$  substrate and thus has 3D character. These electrons most likely originate from extrinsic dopants (oxygen vacancies) throughout the  $\text{SrTiO}_3$  substrate. On the other hand, samples grown and/or annealed at a higher oxygen partial pressure ( $\sim 10^{-4}$  mbar) have conducting electron gases that are quasi-2D, confined within a few (to at most tens of) nanometers of the interface. These results on the thickness of the electron gas are based on a number of methods, including solution of the Poisson equation for the interface system [42], observation of magnetoresistance and Shubnikov-de Hass oscillations at the interface [41], direct imaging using contact-tip atomic force microscopy [57], hard x-ray photoelectron spectroscopy [45], and modeling of the superconducting properties of the interface electron gas [16].

In addition, experiments employing x-ray absorption spectroscopy [46] have been able to furnish information on the orbital character of the electron gas at the  $n$ -type interface. Specifically, the degeneracy of  $t_{2g}$  states (originating from the Ti atom in  $\text{SrTiO}_3$ ) is removed, and the lowest states for conducting electrons are of Ti  $d_{xy}$  character.

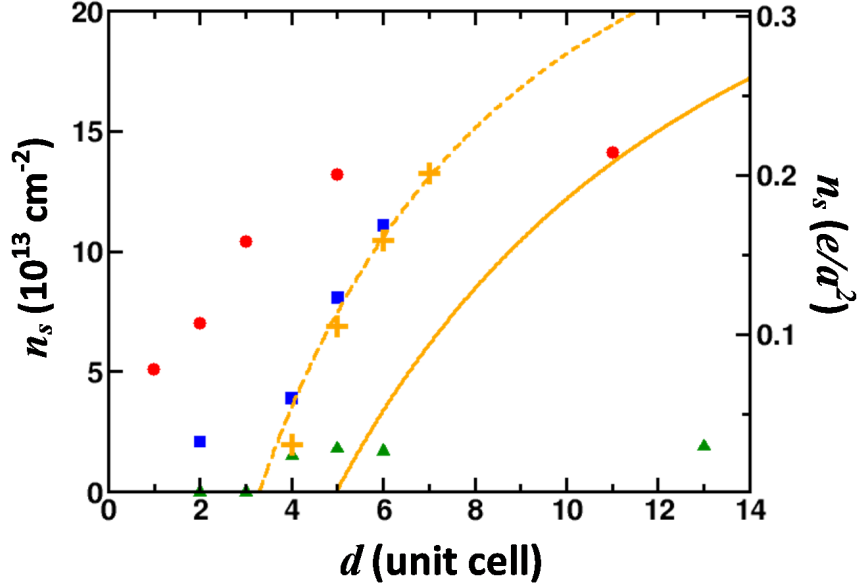


FIG. 2: A comparison of sheet carrier density at the  $n$ -type interface from different published experiments as well as those from first principles theory. The red circles are data from Ref. [55], the blue squares are data from Ref. [45] and the green triangles are data from Ref. [13]. The data from Ref. [55] and Ref. [13] are extracted from transport measurements. The data from Ref. [45] are obtained using hard x-ray photoelectron spectroscopy. Orange pluses are values directly obtained from first principles DFT-LDA calculations. The dashed and solid curves are fits to the first principles data where the  $\text{LaAlO}_3$  is treated as a continuous medium with field dependent dielectric constant (see Sec. III B 1.) The dashed curve is a model using the bulk DFT-LDA band gaps for  $\text{SrTiO}_3$  and  $\text{LaAlO}_3$  whereas the solid curve is corrected for the underestimation of the bulk DFT-LDA band gaps.

### 3. Thickness dependence of sheet carrier density

While it is generally agreed upon that there is a minimum required thickness for the  $\text{LaAlO}_3$  film before mobile carriers and thus conductivity are observed at the  $n$ -type interface, the details of this behavior raise issues yet to be resolved. As with the transport properties, in general, the thickness dependence of  $n_s$  is sensitive to the sample growth conditions. A comparison of the sheet carrier density determined from different available experiments is shown in Fig. 2, along with theoretical predictions from our first principles calculations. (Similar theoretical curves are reported by Son *et al.* [34].)

Thiel *et al.* [13] show that after annealing, the sheet carrier density for samples with fewer than 4 unit cells (u.c.) of  $\text{LaAlO}_3$  is below detectable levels. Above 4 u.c., they observe a step-like jump in  $n_s$ , which then remains in the range of  $1 \times 10^{13} - 2 \times 10^{13} \text{ cm}^{-2}$  and shows no further discernible thickness dependence. The discontinuous jump in sheet density agrees with the polar catastrophe model of the metal-insulator transition, but the value of the sheet density is an order of magnitude smaller than the theoretical value of  $0.5e/a_{\text{STO}}^2$ , or  $3.3 \times 10^{14} \text{ cm}^{-2}$ .

Huijben *et al.* [55] grew *np*-type interface samples with  $p_{\text{O}_2}$  of  $10^{-5}$  mbar without annealing and observe that the samples are conducting for all  $\text{LaAlO}_3$  thicknesses studied:  $n_s$  starts out small but finite for 1 u.c. of  $\text{LaAlO}_3$  and increases with  $\text{LaAlO}_3$  thickness until it saturates at  $1.4 \times 10^{14} \text{ cm}^{-2}$  for  $\geq 6$  u.c. of  $\text{LaAlO}_3$ . As Fig. 2 shows, here the saturation sheet density is closer to the theoretically expected value of  $0.5e/a_{\text{STO}}^2$ , but the carrier density is nonzero and significant for all  $\text{LaAlO}_3$  thicknesses, which is at variance with a metal-insulator transition scenario.

The above results are obtained from transport measurements. Sing *et al.* [45] employ hard x-ray photoelectron spectroscopy to study samples grown under the same conditions as Thiel *et al.* [13] but find that the carrier density is already non-zero for  $\text{LaAlO}_3$  films 2 u.c. thick. In contrast to Ref. [13] but in qualitative agreement with Ref. [55] (despite the differing growth conditions), they observe that  $n_s$  increases with the  $\text{LaAlO}_3$  thickness. The authors propose that the finite sheet carrier density of samples with 2 u.c. of  $\text{LaAlO}_3$  is immobile and does not contribute to transport. This raises the interesting and important question of whether some or all electrons at the *n*-type interface participate in transport, which we further discuss in Section III B 3.

#### 4. Cation disorder and intermixing

Despite the high level of epitaxy available with modern growth techniques, some research groups have observed that significant cation mixing occurs at the *n*-type interface. Nakagawa *et al.* [12], using atomic-resolution electron energy loss spectroscopy (EELS), find that the *n*-type interface is significantly rougher than the *p*-type interface. They suggest that the finite width of the electron gas (as dictated by basic quantum mechanics) increases the electric dipole energy, which in turn is reduced by exchanging Sr with La across the inter-

face. Willmott *et al.* [38] analyze the interface structure using coherent Bragg rod analysis (COBRA) and also observe a graded intermixing over 3 unit cells. In addition, they note that La-Sr mixing is evident for  $\sim 6$  Å further away from the interface than Al-Ti mixing. Since the ionic radii of La and Sr are more than twice as large as those of Al and Ti, the observation of the intermixing is interpreted as a natural tendency of the system, rather than an effect due to kinetic disruption during growth. Overall, the basic mechanisms that are the driving forces for cation disorder require explanation and exploration, as does the question of what procedures can effectively reduce such intermixing to create ideal interfaces.

### 5. *Magnetic properties*

Experimental studies of the magnetic properties of the *n*-type interface are an active and growing area. To date, some intriguing discoveries have been reported by various research teams based on using magnetoresistance measurements as an indirect probe of magnetic behavior and ordering. Measurements by Brinkman *et al.* [19] provide the first experimental evidence of magnetic behavior. Since then, additional studies [58, 59] suggest that some type of magnetic ordering may occur at low temperatures. However, there are still questions about whether the system exhibits hysteretic behavior, the sign of the magnetoresistance, and whether the magnetoresistance is isotropic or anisotropic.

Brinkman *et al.* [19] studied samples grown under a relatively high  $p_{\text{O}_2} \sim 10^{-3}$  mbar, with sheet resistances  $> 10^4$  Ω. They observe isotropic magnetoresistance, which they ascribe to spin scattering off localized magnetic moments at the interface, an interpretation bolstered by their observation of a minimum in the sheet resistance  $R_s(T)$  with lowering temperature. This minimum is reminiscent of the Kondo effect, which stems from the interplay between localized magnetic moments and itinerant charges. Furthermore, they find that the magnetoresistance at 300 mK is hysteretic, implying the presence of ferromagnetic domains. However, the  $R_s(T)$  minimum is not present for samples grown at lower  $p_{\text{O}_2}$  ( $< 10^{-5}$  mbar). In contrast, Reyren *et al.* [16] grew a sample at a low oxygen partial pressure of  $6 \times 10^{-5}$  mbar, which is then annealed under conditions that (presumably) yield well oxidized samples. They find positive magnetoresistance, no minimum in  $R_s(T)$ , and no hysteresis in magnetoresistance. The two major differences between the experiments of Refs. [19] and [16] are the growth  $p_{\text{O}_2}$  ( $10^{-3}$  mbar versus  $10^{-5}$  mbar) and the thickness of the

LaAlO<sub>3</sub> film (26 u.c versus 8 u.c.). The former factor is known to affect the sheet resistance and mobility, while the latter modifies the sheet carrier density.

The SrTiO<sub>3</sub>/LaAlO<sub>3</sub> samples investigated by van Zalk *et al.* [58] are grown under similar conditions to those used by Brinkman *et al.* [19]. This study reports hysteresis below 300 mK and magnetoresistance oscillations versus external field intensity  $B$  at 50 mK. Surprisingly, the oscillations are periodic in  $\sqrt{B}$  instead of the standard Shubnikov-de Haas  $1/B$  periodicity. The authors suggest that this stems from the commensurability condition of edge states. They also speculate that the magnetoresistance oscillation is related to ferromagnetic ordering, and that the quantum Hall effect might be present.

Shalom *et al.* [59] studied samples grown at a lower  $p_{\text{O}_2}$  of  $10^{-4} - 10^{-5}$  mbar. In agreement with other observations [13, 16, 40], the sheet carrier density is  $\sim 10^{13}$  cm<sup>-2</sup> and the system becomes superconducting at 130 mK. In contrast to Refs. [19] and [58], however, the low temperature magnetoresistances are highly anisotropic and have different signs for fields parallel or perpendicular to the current. They find no hysteresis down to 130 mK, at which point their samples become superconducting. Based on these observations, they suggest an anti-ferromagnetic ordering at the interface below a Néel temperature of  $\sim 35$  K.

## B. The $p$ -type interface

Experimentally, the  $p$ -type interface (AlO<sub>2</sub>/SrO) is less explored than the  $n$ -type interface. Nakagawa *et al.* [12] suggest that the insulating properties of the  $p$ -type interface arise from the presence of oxygen vacancies. Unlike the  $n$ -type interface, at which the Ti can exist in multiple valence states, the  $p$ -type interface has no multi-valent element (*e.g.*, O<sup>-</sup> is very unusual in compounds). Hence, they argue that, in order to compensate the internal polar field and potential across the LaAlO<sub>3</sub> film, an atomic reconstruction such as a high density of oxygen vacancies is required.

In a simple ionic picture, an ideal and unreconstructed  $p$ -type interface has 0.5 holes per interface unit cell to compensate the polar field in the LaAlO<sub>3</sub> film. An oxygen vacancy can potentially donate two electrons, and assuming that both electrons are mobile, a density of one oxygen vacancy per four two-dimensional (2D) interface unit cells can precisely accommodate the holes and leave no carriers at the  $p$ -type interface. Using atomic resolution EELS and various fitting procedures, Nakagawa *et al.* [12] infer the presence of  $0.32 \pm 0.06$

oxygen vacancies per 2D unit cell in the SrTiO<sub>3</sub> near the *p*-type interface, which is three times higher than their inferred value of 0.1 oxygen vacancies per 2D unit cell at the *n*-type interface.

Although these results support the oxygen vacancy picture, they also raise some questions. The first issue is whether both electrons on the oxygen vacancy are in fact *mobile* and hence can be donated to the interface. The experimental finding of 0.32 oxygen vacancies per 2D unit cell argues that more than 0.25 oxygen vacancies per 2D unit cell are needed. There is also theoretical evidence to support this incomplete donation of electrons [25], a subject we return to in Section III C 3.

Regardless of the precise number of oxygen vacancies, in the polar catastrophe scenario the holes are created by  $0.5e/a_{\text{STO}}^2$  electrons being transferred away from the *p*-type interface to the other side of the LaAlO<sub>3</sub> film, whether it be the LaAlO<sub>3</sub> surface or another *n*-type interface with a capping layer. Why do these electrons make no contribution to the transport? This question also applies to the *n*-type and *np*-type interfaces, which similarly should have holes on the LaAlO<sub>3</sub> surface or at the capping *p*-type interface, but experimentally show only electron-like carriers in transport. We discuss this point further in Section IV C below.

In summary, though the *n*-type interface has interesting properties that are promising for potential applications, understanding the *p*-type interface is equally important from a theoretical point of view.

### III. FIRST PRINCIPLES THEORY

In this section, we focus on the theoretical work on the SrTiO<sub>3</sub>/LaAlO<sub>3</sub> interface system. Most of the theoretical literature is devoted to elucidating the origin of the conducting electron gas, reproducing the insulating-to-metallic transition, and designing new interfaces with more interesting properties. Some successes have been achieved in the comparison between theory and experiment. However, discrepancies exist and some important questions are unresolved. Although some interesting results have been obtained from model Hamiltonian calculations [60], we concentrate here on first principle calculations.

## A. Theoretical methodologies

With few exceptions, most first principles studies of SrTiO<sub>3</sub>/LaAlO<sub>3</sub> interfaces to date have focused on defect-free and idealized *n*-type and *p*-type interfaces. Aside from the desire to understand the basic physics and intrinsic properties of high quality interfaces, the primary practical reason has been due to computational costs: including imperfections such as oxygen vacancies, cation intermixtures, or other atomic reconstructions requires the use of relatively large simulation cells. Theoretical studies reporting on oxygen vacancies include Refs. [21, 24, 25, 32] with one work on modeling intermixing [38]. However, understanding the ideal interfaces is both a good starting point for gaining theoretical insight and should also be relevant to experiments where it is believed that high quality interfaces have been achieved.

Most of the reported calculations use density functional theory (DFT) [61] with the local density approximation (LDA) [61] or the generalized gradient approximation (GGA) [62]. A subset have employed the LDA+*U* method to include approximately some effects of localized electronic correlations that are missing from standard LDA or GGA DFT calculations [63]. This has been done typically by including Hubbard *U* and exchange *J* corrections on the Ti-*d* manifold, although Pentecheva and Pickett [24] apply *U* on the oxygen *p* orbitals to study the possibility of hole polarons at the *p*-type interface. The *U* values employed and the resulting predictions are not unanimous, ranging from 5 eV to 8 eV [24, 27–29, 64]. In particular, Zhong and Kelly [29] studied the *n*-type interface properties as a function of *U* ranging from 0 to above 6 eV and find a variety of geometric, electronic, and magnetic ground states versus *U*.

The simulation cells used fall into three distinct categories, which provide complementary information on these interfaces. The most popular approach has been to employ a symmetric superlattice: a number of unit cells of SrTiO<sub>3</sub> are placed next to a number of unit cells of LaAlO<sub>3</sub> along (001) and periodic boundary conditions are applied. In this symmetric superlattice approach, both the SrTiO<sub>3</sub> and LaAlO<sub>3</sub> films are nonstoichiometric: when the SrTiO<sub>3</sub> has an additional TiO<sub>2</sub> atomic layer and the LaAlO<sub>3</sub> has an extra LaO layer, two identical *n*-type interfaces are formed to make a symmetric system (Fig. 3a); extra SrO and AlO<sub>2</sub> layers create two *p*-type interfaces (Fig. 3c). The symmetric superlattice allows for simulation of a single interface type in isolation, and leads to relatively small simulation cells.

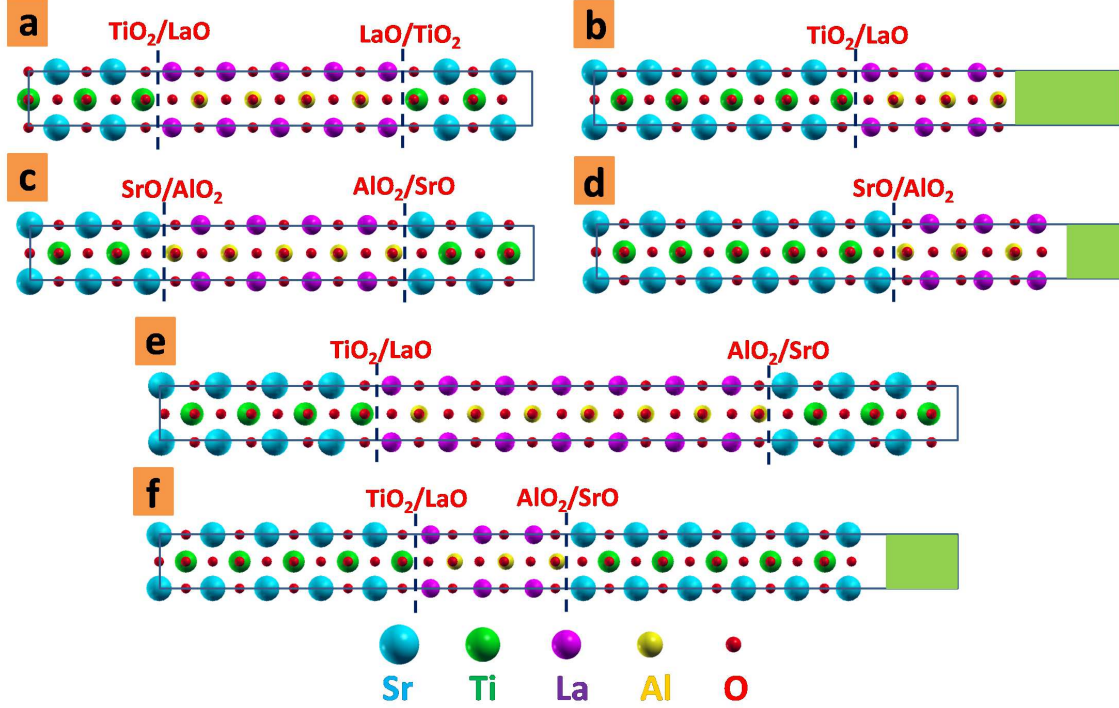


FIG. 3: Schematics of simulation cells for various types of interfaces and superlattices for the  $\text{SrTiO}_3/\text{LaAlO}_3$  system. The shaded green regions denote vacuum; their thickness is merely schematic and not indicative of actual thickness used in the simulation. For superlattice simulations, there is no vacuum in the unit cell. For interface simulations, the vacuum is inserted to separate periodic copies and introduce surfaces. **a)**  $n$ -type superlattices, **b)**  $n$ -type interfaces, **c)**  $p$ -type superlattices, **d)**  $p$ -type interfaces, **e)**  $np$ -type superlattices and **f)**  $np$ -type interfaces.

However, due to the imposed symmetry and the lack of stoichiometry, the  $\text{LaAlO}_3$  film is nonpolar. This precludes the study of the polar catastrophe and the evolution of the interface properties as a function of  $\text{LaAlO}_3$  thickness. Due to the nonstoichiometry, one additional electron (for double  $n$ -type) or one additional hole (for double  $p$ -type) is introduced into the symmetric supercell, which means essentially 0.5 carriers per 2D interface unit cell are doped at each interface in the calculation, *i.e.*, the sheet carrier density is fixed as dictated by chemistry. Physically, 0.5 carriers per 2D cell is the required amount to completely compensate the  $\text{LaAlO}_3$  polar field [12], meaning that the symmetric supercell approach provides the properties of the interfaces in the thick  $\text{LaAlO}_3$  film limit.

Experimental growth procedures generate stoichiometric  $\text{LaAlO}_3$  and  $\text{SrTiO}_3$  films that are thin (on the order of nanometers) and often have exposed oxide surfaces or capping layers.

Therefore, the next generation of computations employs simulation cells with stoichiometric films and regions of vacuum to break periodic boundary conditions along (001), as illustrated in Fig. 3b, 3d, and 3f. The presence of a vacuum region in the simulation cell allows for the polar potential developed through the  $\text{LaAlO}_3$  film to drop across the vacuum gap instead of through the materials themselves. To simulate the stoichiometric interfaces, a slab of  $\text{SrTiO}_3$  is typically used to model the substrate, a  $\text{LaAlO}_3$  film is placed on this slab, and, depending on the system being modeled, the  $\text{LaAlO}_3$  can terminate at the vacuum or a further capping film is added on top of the  $\text{LaAlO}_3$ . In the first case, the system has a single buried  $n$ -type (Fig. 3b) or  $p$ -type (Fig. 3d) interface with an exposed surface; in the second case, a pair of  $n$ -type and  $p$ -type interfaces coexist on the two sides of the  $\text{LaAlO}_3$  film. We refer to these system as the  $n$ -type,  $p$ -type, and  $np$ -type interfaces, respectively. (We note that all three types have been fabricated in experiments.) These stoichiometric simulations have a polar  $\text{LaAlO}_3$  film with an internal field going from the  $(\text{LaO})^+$  to  $(\text{AlO}_2)^-$  terminating atomic layers. Therefore, such simulations can probe the evolution of the polar catastrophe and sheet carrier properties with  $\text{LaAlO}_3$  thickness. Furthermore, assuming ideal interfaces and surfaces, these calculations represent a faithful reproduction of many of the actual experiments. Due to the close proximity of the exposed surfaces to the interfaces, the effect of surface defects or adsorbates on the interface properties can also be investigated.

Finally, there is another type of geometry employed in simulations [23, 25, 26, 65], which we refer to as  $np$ -type superlattices (Fig. 3e). These superlattices have stoichiometric  $\text{SrTiO}_3$  and  $\text{LaAlO}_3$  but do not include vacuum. The absence of vacuum makes the electronic structures of  $np$ -type superlattices different from those of  $np$ -type interfaces (Fig. 3f), as we discuss in more detail in Section III B 1 with more details.

## B. The $n$ -type interface

In this subsection, we review the state-of-art theoretical results from first principles simulations of  $n$ -type and  $np$ -type interfaces, as well as double  $n$ -type and  $np$ -type superlattices.

### 1. Critical separation

As discussed above, an insulating-to-metallic transition has been observed at the SrTiO<sub>3</sub>/LaAlO<sub>3</sub> interface for LaAlO<sub>3</sub> films thicker than 4 u.c. [13]. The polar nature of LaAlO<sub>3</sub> provides an explanation for this behavior, *i.e.* the polar catastrophe. This transition can be understood by considering the SrTiO<sub>3</sub>/LaAlO<sub>3</sub> energy band diagram. The energy diagram of the *n*-type interface is shown in Fig. 4b. Drawn schematically on the left side are the valence and conduction band edges of the SrTiO<sub>3</sub> substrate, which are composed of O *p*- and Ti *d*-states, respectively. To the right are the LaAlO<sub>3</sub> band edges, which are composed of O *p*- and La *d*-states, respectively. Due to the polar nature of LaAlO<sub>3</sub>, there is an electric field through the stoichiometric LaAlO<sub>3</sub> film. Consequently, the bands slope up linearly inside the LaAlO<sub>3</sub> film. The upwards slope in Fig. 4b indicates that the positively charged (LaO)<sup>+</sup> layer at the *n*-type interface attracts electrons. As the figure illustrates, the energy gap of the entire *n*-type interface system is determined by the difference between conduction band edge Ti *d*-states of the SrTiO<sub>3</sub> substrate and the valence band edge O *p*-states at the LaAlO<sub>3</sub> surface. Each added LaAlO<sub>3</sub> unit cell increases the surface valence band edge by approximately a fixed amount, thereby reducing the total energy gap of the entire interface system. The smallest thickness of LaAlO<sub>3</sub> that closes the energy gap is thus the critical separation at which the system becomes metallic. Fig. 4a shows that the *np*-type interface behaves similarly, although in this case the total energy gap is determined by the conduction band edge Ti *d*-states of the SrTiO<sub>3</sub> substrate and the valence band edge O *p*-states in the capping SrTiO<sub>3</sub> layer.

The insulating-to-metallic transition has been directly confirmed by DFT studies on stoichiometric interfaces such as those shown in Fig. 3b and 3f [28, 32–34]. By computing local densities of states in each atomic plane, it is straightforward to locate the band edges and to recreate energy band diagrams of the style shown in Fig. 4a and 4b. These diagrams show precisely the behavior described above.

While the theoretically predicted and experimentally observed values for the critical separation are similar, they are not in quantitative agreement. From the discussion above, one can see that the value of the critical separation depends on the band gap of SrTiO<sub>3</sub>. As is well known, band gaps are systematically underestimated in DFT calculations. Nevertheless, direct comparison with experiment can be achieved by including a manual correction to the

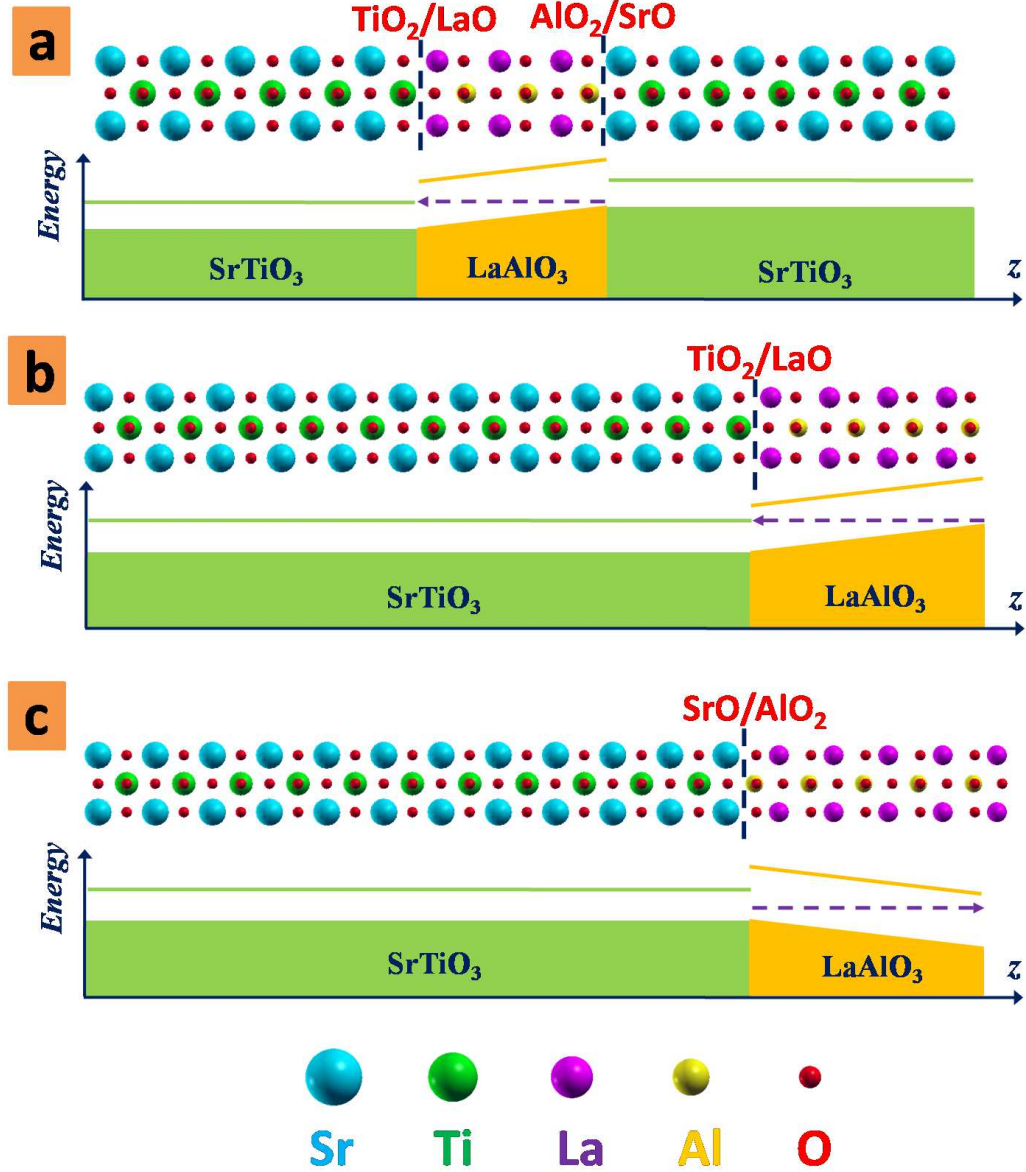


FIG. 4: Schematic of energy diagrams for a)  $np$ -type, b)  $n$ -type and c)  $p$ -type interfaces, respectively. The shaded parts are filled valence bands. The conduction bands are empty, and their edges are denoted by the solid lines. The dashed arrow refers to the direction of charge transfer.

band gap, which physically amounts to adding 1 or 2 unit cells of  $\text{LaAlO}_3$  to the theoretical critical separation. In previous work [32], we employ LDA to study the critical separation of the  $n$ -type and  $np$ -type interfaces. We determine that the increase of the potential with each added  $\text{LaAlO}_3$  unit cell is  $\simeq 0.7$  eV, which corresponds to an average electric field of  $0.19$  V/Å in the  $\text{LaAlO}_3$  film prior to the polar catastrophe. The band gap of  $\text{SrTiO}_3$  in

our calculations is 1.9 eV. Taking into account the difference between this and the experimental SrTiO<sub>3</sub> band gap of 3.2 eV, we predict that the experimental critical separation is 6 and 5 LaAlO<sub>3</sub> u.c. for the *n*-type and *np*-type interfaces, respectively. Using GGA with a similarly underestimated SrTiO<sub>3</sub> band gap of 2.0 eV, Pentcheva and Pickett [33] predict a critical separation of greater than 6 unit cells for the *n*-type interface based on a potential shift of 0.4 eV per added LaAlO<sub>3</sub> unit cell. Cen *et al.* [21] find similar values as well: using GGA calculations with a SrTiO<sub>3</sub> band gap of 1.8 eV, they find the theoretical critical separation of the *n*-type interface to be 4 u.c. of LaAlO<sub>3</sub> and predict that the experimental critical separation should be larger than this value. Therefore, for ideal *n*-type interfaces and polar LaAlO<sub>3</sub> films, LDA and GGA-based DFT calculations have reached a consensus that the critical thickness is larger than 4 unit cells and is most likely 6 unit cells for the *n*-type interface.

Comparison to experiment is complicated by the experimental variances discussed in the previous section. The theoretical predictions are larger than the experimental value of 4 u.c. of Thiel *et al.* [13] as determined by transport, or even 2 u.c. from hard x-ray spectroscopy results of Sing *et al.* [45] for *n*-type interfaces with exposed LaAlO<sub>3</sub> surfaces. For the buried *np*-type interfaces studied by Huijben *et al.* [55], the comparison is better in the sense that the sheet carrier density saturates for LaAlO<sub>3</sub> films 6 u.c. thick. However, those experiments find finite carrier densities even for 1 u.c. of LaAlO<sub>3</sub>, in disagreement with the metal-insulator transition scenario.

At the LDA+U level, Lee and Demkov [28] use a Hubbard correction on the Ti *d* manifold with  $U=8.5$  eV to shift the conduction band edge of SrTiO<sub>3</sub> and increase its band gap to 3.2 eV. They report a stronger polar field of 0.24 V/Å. They simulate three and five u.c. thick LaAlO<sub>3</sub> films and find that the five unit cell case undergoes an metal-insulator transition. Therefore, they report a smaller critical separation of 4 or 5 LaAlO<sub>3</sub> unit cells. This value is closer to the experimental one determined from transport measurements on the *n*-type interface with exposed LaAlO<sub>3</sub> surfaces of Ref. [13] but differs from the other two experiments.

We note that in all the above simulations, the LaAlO<sub>3</sub> film itself is modeled using standard LDA or GGA methodologies. Therefore, *prima facie* it is not clear why there is a spread of predicted polar fields since the polar field is a property of the LaAlO<sub>3</sub> film itself. To shed some light on this issue of variations in the theoretical predictions, we remark that it is

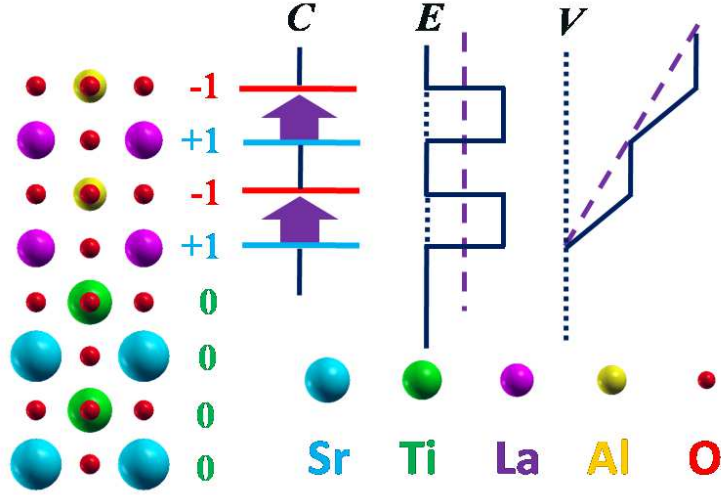


FIG. 5: Schematic showing how an  $\text{LaAlO}_3$  film can be approximated as a series of parallel-plate capacitors and the resulting distribution of electric field and potential. The solid lines refer to the actual electric field and potential generated by the capacitors. The dashed lines are the averaged electric field and potential over each unit cell.

possible to make an *a priori* estimate of the polar field in  $\text{LaAlO}_3$  using only bulk properties of the material. Denoting the lattice constant of  $\text{LaAlO}_3$  as  $a_{\text{LAO}}$ , the  $\text{LaAlO}_3$  atomic planes along (001) are alternately  $(\text{LaO})^+$  and  $(\text{AlO}_2)^-$  and separated by a distance of  $a_{\text{LAO}}/2$ . A simple parallel plate model can be made, as illustrated in Fig. 5. The  $\pm e/a_{\text{STO}}^2$  surface charge on each plane is spread over a  $\text{SrTiO}_3$  unit cell area  $(a_{\text{STO}})^2$  and the resulting electric fields are screened by the  $\text{LaAlO}_3$  dielectric constant,  $\epsilon_{\text{LAO}}$ . Since the field only acts in half of each unit cell, we have for the potential energy change  $\Delta V$  across a unit cell

$$\Delta V = \frac{a_{\text{LAO}}}{2} \cdot \frac{4\pi e^2}{\epsilon_{\text{LAO}}(a_{\text{STO}})^2} \quad (1)$$

or converting to the average internal polar electric field

$$E_{\text{polar}} = \frac{2\pi e}{\epsilon_{\text{LAO}}(a_{\text{STO}})^2} \quad (2)$$

Using experimental values of  $a_{\text{STO}} = 3.905 \text{ \AA}$ ,  $a_{\text{LAO}} = 3.789 \text{ \AA}$ , we have

$$\Delta V = \frac{22.5 \text{ eV}}{\epsilon_{\text{LAO}}} \quad , \quad E_{\text{polar}} = \frac{5.94 \text{ V/\AA}}{\epsilon_{\text{LAO}}} \quad (3)$$

Therefore, each calculation of  $\Delta V$  or  $E_{\text{polar}}$ , and thus the resulting critical separation, can be directly mapped to a value of  $\epsilon_{\text{LAO}}$  implicit in the calculation.

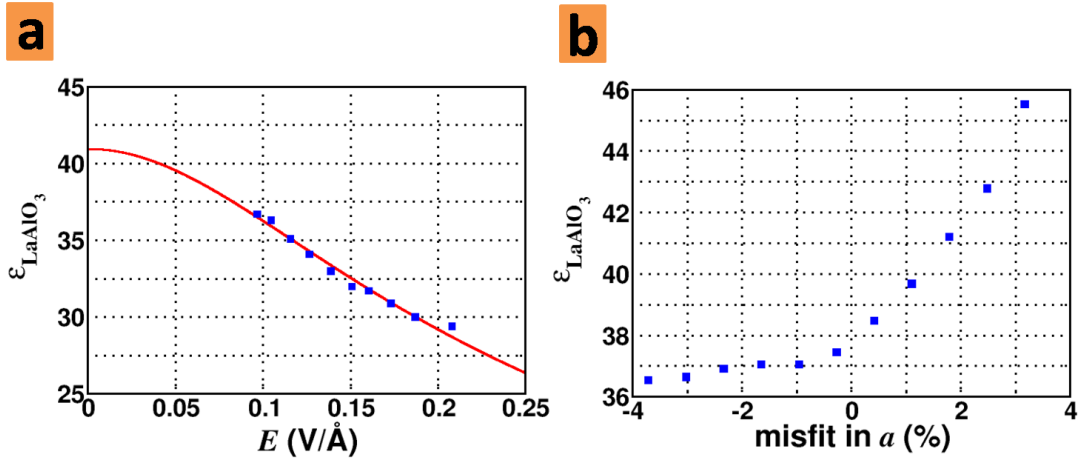


FIG. 6: **a)** Electric field dependence of the bulk  $\text{LaAlO}_3$  dielectric constant. The solid line is a fit to the first principles calculation, using the Landau-Devonshire formalism Eq. (4) [66] with  $\epsilon_0 = 40.95$  and  $E_0 = 0.15 \text{ V/\AA}$ . **b)** Strain dependence of the  $\text{LaAlO}_3$  dielectric constant. The internal electric field is set to be  $0.026 \text{ V/\AA}$  (weak enough that the  $\text{LaAlO}_3$  remains insulating). The  $c/a$  ratio is optimized for each  $a$ . The strain is measured with respect to the theoretically predicted lattice constant of  $\text{SrTiO}_3$  (in experiments the  $\text{LaAlO}_3$  film is coherently strained to the  $\text{SrTiO}_3$  substrate).

In Table II, we compile the published values of  $\Delta V$  or  $E_{polar}$  and back out  $\epsilon_{\text{LAO}}$  as per Eq. (3). As expected, larger  $\Delta V$  or  $E_{polar}$  lead to smaller predicted critical separations, as well as smaller implied  $\epsilon_{\text{LAO}}$ . The range of  $\epsilon_{\text{LAO}}$  spans a factor of more than two, which raises the question of why the spread is so large.

The actual value of the dielectric constant of  $\text{LaAlO}_3$  depends on the strain state and internal electric field in the material, as well as technical choices such as the pseudopotential and basis set (a similar dependence study of  $\epsilon_{\text{STO}}$  is presented in [67]). We present the field and strain dependence of  $\epsilon_{\text{LAO}}$  for bulk  $\text{LaAlO}_3$  in Fig. 6a and 6b. The field dependence is calculated in a slab geometry because only thin films can accommodate large internal electric fields of around  $0.2 \text{ V/\AA}$  without becoming metallic. The dependence can be described phenomenologically using the Landau-Devonshire formalism [66] (the solid line in Fig. 6a), which yields, approximately:

$$\epsilon(E) \simeq \epsilon_0 \left( 1 + \left( \frac{E}{E_0} \right)^2 \right)^{-1/3} \quad (4)$$

TABLE II: Polar properties of LaAlO<sub>3</sub> films and  $n$ -type interfaces from first principles calculations. Values of the potential change per added LaAlO<sub>3</sub> unit cell  $\Delta V$  and the polar field  $E_{polar}$  are related by Eq. (3). In each reference, only one of the two values is reported. The same equation then provides the dielectric constant  $\epsilon_{LAO}$ .

$\Delta V$ (eV)	$E_{polar}$ (V/Å)	Estimated critical separation	$\epsilon_{LAO}$	Reference
0.4	0.1	>6	56	Pentcheva and Pickett [33]
0.6	0.16	>4	38	Cen <i>et al.</i> [21]
0.7	0.19	6	32	Chen <i>et al.</i> [32]
0.8	0.2	5	30	Son <i>et al.</i> [34]
0.91	0.24	4 to 5	25	Lee and Demkov [28]

where  $\epsilon_0$  and  $E_0$  are two fitting parameters.

In addition,  $\epsilon_{LAO}$  is affected by the strain state of the LaAlO<sub>3</sub> film, which is in epitaxial relation to the SrTiO<sub>3</sub> substrate. The strain dependence versus in-plane lattice constant is calculated using the Berry phase method [68] with a weak internal electric field (0.026 V/Å) so that the system remains insulating and the polarization as a response to the external electric field is in the linear region. The  $c$ -axis is optimized for each choice of  $a$ -axis parameter. The data in Fig. 6 show that  $\epsilon_{LAO}$  is sensitive to the in-plane strain and the internal electric field of the LaAlO<sub>3</sub> film. Both properties depend on technical choices: *e.g.*, different choices of basis sets and/or pseudopotentials change the lattice constant of SrTiO<sub>3</sub> by  $\pm 1$ -2%, which appears to be a minor difference but in fact has a significant effect on  $\epsilon_{LAO}$ . We believe that a large part of the theoretical spread is caused by these sensitivities.

To summarize, theoretical work to date has shown that the polar catastrophe mechanism does indeed predict a critical separation for  $n$ -type and  $np$ -type interfaces. Furthermore, reasonable values of 5-6 unit cells of LaAlO<sub>3</sub> are found. The well known underestimation of band gaps from LDA or GGA means that the actual critical separations must be larger than the raw values produced by such approaches. That the predicted critical separations are larger than those found in most, but not all, experiments suggests that other mechanisms may play a role before or in conjunction with the polar catastrophe.

Before concluding the discussion of the critical separation, we mention that an insulating-

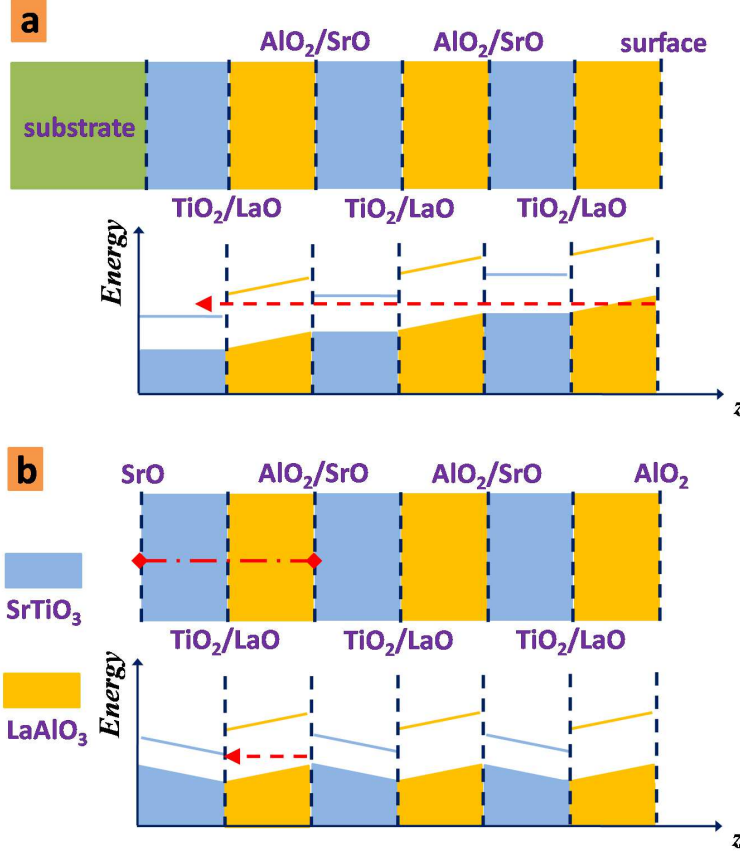


FIG. 7: **a)** The experimental stoichiometric  $np$ -type superlattice and its corresponding energy diagram. The electrostatic potential is stair-like. **b)** The theoretical stoichiometric  $np$ -type superlattice with periodic boundary conditions and no vacuum region, and its corresponding energy diagram. Due to periodic boundary conditions, the potential has a zigzag shape. The unit cell for the periodic boundary conditions is illustrated by the red dot-dash line. In both cases, dashed lines with arrows show the direction of electron transfer when the polar catastrophe occurs in each system.

to-metallic transition is also recently found in the simulations of  $np$ -type superlattices with no vacuum regions [65]. We would like to point out that there is a subtle difference between experimental and simulated  $np$ -type superlattices (illustrated in Fig. 7). For an experimental  $np$ -type superlattice, the films are of finite size, terminate at surfaces, and are not subject to periodic boundary conditions. For such systems, a “global” insulating-to-metallic transition can occur, which is missing in simulations with enforced periodic boundary conditions. As per Fig. 7a, before any electronic reconstructions takes place, the energy diagram of an

experimental  $np$ -type superlattice is stair-like: the potential is constant in the nonpolar SrTiO<sub>3</sub> and increases linearly in the polar LaAlO<sub>3</sub> layers. When the superlattice is thick enough, the electrons filling the LaAlO<sub>3</sub> valence bands on the surface tunnel into the empty conduction bands of SrTiO<sub>3</sub> substrate. This is the “global” insulating-to-metallic transition as the transferred electrons and holes generate an additional internal electric field throughout the *entire* superlattice. This additional field counteracts the polar field of LaAlO<sub>3</sub> film and distorts the electrostatic potential, as illustrated in Fig. 7b. Thus the limit of infinitely thick experimental  $np$ -type superlattices can be simulated by imposing periodic boundary conditions imposed on one superlattice unit cell. Separately, if one increases the thickness of the LaAlO<sub>3</sub> film in each periodic unit, there will be a “local” insulating-to-metallic transition in which electrons in the LaAlO<sub>3</sub> valence states tunnel into the SrTiO<sub>3</sub> conduction bands in the *same* unit superlattice. We note that the “global” transition (in experiment) or the periodic boundary conditions (in computation) generates a counteracting field that polarizes the SrTiO<sub>3</sub> and reduces the polar field in the LaAlO<sub>3</sub> film. This explains the smaller value of 0.057 V/Å[65] obtained in this approach. In earlier calculations using relatively small unit cells [23, 25, 26], the theoretical  $np$ -type superlattices turn out to be insulating at LaAlO<sub>3</sub> thicknesses that make the  $np$ -type interface metallic. By employing much thicker films in the superlattice unit cell (12 u.c. of SrTiO<sub>3</sub> and LaAlO<sub>3</sub> ) an insulating-to-metallic transition is found [65], and as expected from the above reasoning the critical separation of  $np$ -type superlattices is quite a bit larger than that of  $np$ -type interfaces.

## 2. Orbital character of interface bands

In both simulations [24, 30, 32, 34] and experiments [46], it has been seen that the Ti-derived  $t_{2g}$  degeneracy is split at the  $n$ -type interface. Theoretical studies show that the lowest occupied bands at the interface reside primarily in the SrTiO<sub>3</sub> and have a clear Ti  $d_{xy}$  character. With increasing energy (or equivalently, sheet carrier density),  $d_{xz}$  and  $d_{yz}$  derived states also become partially occupied. Therefore, for all but the very lowest sheet carrier densities, multiple interfacial bands, with possibly different orbital character, are occupied.

Detailed band structures for the  $n$ -type interface have been presented in Refs. [30, 34] with some differences. Popović *et al.* [30] use a symmetric double  $n$ -type superlattice, which

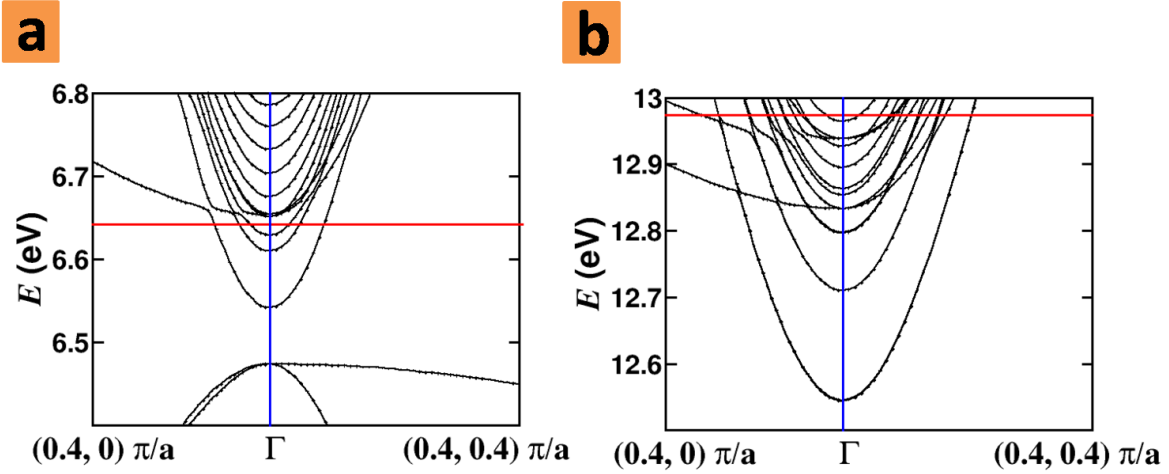


FIG. 8: The band structures of an  $n$ -type interface and an  $n$ -type superlattice from DFT-LDA calculations. The solid horizontal red line is the Fermi level. **a)**  $n$ -type interface with 11 u.c. of SrTiO<sub>3</sub> and 5 u.c. of LaAlO<sub>3</sub>. The thickness of vacuum separating periodic copies is more than 30 Å. The sheet carrier density is  $0.1e/a_{\text{STO}}^2$ . **b)**  $n$ -type symmetric superlattice with 12.5 u.c. of SrTiO<sub>3</sub> (with extra TiO<sub>2</sub> plane) and 4.5 u.c. of LaAlO<sub>3</sub> (and extra LaO plane). As described in the text, the sheet carrier density is forced to be  $0.5e/a_{\text{STO}}^2$ .

enforces the presence of precisely  $0.5e/a_{\text{STO}}^2$  at each  $n$ -type interface (equivalent to what would be found for a very thick LaAlO<sub>3</sub> film). Son *et al.* [34] use a stoichiometric  $n$ -type interface calculation and present the band structure for 5 u.c. of LaAlO<sub>3</sub>, which gives rise to  $0.2e/a_{\text{STO}}^2$  at the interface. The energy difference between the lowest and next lowest interface band edges, both of  $d_{xy}$  character, is 0.1 eV when  $0.2e/a_{\text{STO}}^2$  is present at the interface, but this value triples to 0.3 eV when  $0.5e/a_{\text{STO}}^2$  is transferred. In other words, there is an evolution of the energy spacings of interface states as a function of electron doping. Both works show that the lowest  $d_{xy}$  band is localized in the (001) direction and thus can be said to have a strong two-dimensional (2D) character. Higher energy interface bands extend further into the SrTiO<sub>3</sub> substrate in the (001) direction and are thus more 3D in character.

A convenient way to summarize some of these facts is to show the Fermi surface of the interface system in the  $k_x, k_y$  interface plane. Fig. 8 shows such a diagram. Following the above discussion, the lowest energy  $d_{xy}$  band has the largest occupancy and thus the largest Fermi surface. With increasing energy, the bands have smaller Fermi surfaces.

### 3. Possibility of Anderson localization

Discrepancies between theoretical predictions and experimental measurements of the sheet carrier density [13] have stimulated discussion as to whether all of the transferred electrons contribute to the conductivity [30, 34]. An appealing argument for carriers to have different mobilities, first proposed by Popović *et al.* [30], is based on the fact that, formally, all electronic states in 2D are Anderson-localized by disorder in the thermodynamic limit. Since contributions of localized states to transport are greatly suppressed, the idea is that electrons occupying 2D-like states should have a stronger tendency to localize and therefore not contribute to transport.

Popović *et al.* argue that the lowest  $d_{xy}$  band, which is strongly bound to the interface, should therefore be ignored in predictions of the transport carrier density. Furthermore, they contend that the higher energy bands with  $d_{xz}$  or  $d_{yz}$  character should also localize because they have large effective masses along the (100) or (010) directions. The only electronic states that should contribute to transport are the higher-lying  $d_{xy}$  bands. They determine the carrier density from these bands to be  $8 \times 10^{13} \text{ cm}^{-2}$ , which is closer to, but still a few times larger than, the carrier density measured by Thiel *et al.* [13]. The results of Huijben *et al.* [55], however, show a *larger* value of  $1.4 \times 10^{14} \text{ cm}^{-2}$ .

Son *et al.* [34] take this analysis one step further. They exclude the lowest  $d_{xy}$ ,  $d_{xz}$ , and  $d_{yz}$  bands as well as any  $d_{xy}$  bands whose wave function is concentrated within  $\sim 2 \text{ nm}$  of the interface, under the assumption that such electrons are easily scattered by interface roughness and therefore have low mobility. Only electrons occupying loosely bound or unbound  $d_{xy}$  bands are counted as contributing to transport. They find a sheet carrier density that agrees well with the transport data from Ref. [13] (but not that from Ref. [55]) in that it has a discontinuous jump at a critical thickness and then quickly saturates to a value of  $\sim 2 \times 10^{13} \text{ cm}^{-2}$ .

We suggest that a direct experimental test of such localization would be to deliberately modify the amount of disorder by growing the same interface system with variable quality. Localization would show up as a variation in the transport carrier density. In the absence of such data, however, we attempt to estimate theoretically the necessary conditions for the likelihood of the Anderson localization scenario at the non-interacting, one-particle level. We follow the review by Lee and Ramakrishnan [69].

In 2D, all eigenstates of an infinitely large disordered system are localized: any eigenfunction  $\psi(\mathbf{r})$  will behave as  $|\psi(\mathbf{r})| \sim \exp(-|\mathbf{r} - \mathbf{r}_0|/\xi)$ , where  $\mathbf{r}_0$  is the site about which the state is localized and  $\xi$  is the localization length. To understand the consequences of this for a finite system, the scaling theory of localization [70] describes the evolution of the sample conductance,  $G(L)$ , as the length scale  $L$  evolves from microscopic to macroscopic dimensions. Localization suppresses the conductance, so that when  $L > \xi$ ,

$$G(L) \sim \frac{e^2}{\hbar} \exp(-L/\xi). \quad (5)$$

For SrTiO<sub>3</sub>/LaAlO<sub>3</sub> interfaces, the theoretical asymptotic sheet density is  $0.5e/a_{\text{STO}}^2$ , or  $3.3 \times 10^{14} \text{ cm}^{-2}$ . In order to match transport experiments that give  $2 \times 10^{13} \text{ cm}^{-2}$ ,  $\sim 90\%$  of the electrons must be localized. Their contribution to the conductance must be at least 100 times smaller than the remaining  $\sim 10\%$ . Thus, a conservative bound is  $\exp(L/\xi) > 100$  or  $L/\xi > 4.6$ . In a typical experiment, the contacts used for transport measurements can be about 1 mm apart [13], setting another conservative upper bound of  $L = 1 \text{ mm}$ , meaning  $\xi < 0.2 \text{ mm}$ .

The scaling theory also provides estimates for  $\xi$ . For the weak scattering scenario,  $\xi$  is of order

$$\xi \sim l \exp\left(\frac{\pi}{2} k_F l\right) \quad (6)$$

where  $k_F$  is the Fermi wave vector of the electrons being considered and  $l$  is the mean free path. (Weak scattering is defined as  $k_F l \gg 1$ .) The DFT band structures in Fig. 8, which are similar to the results of Refs. [30, 34], provide us with  $k_F$  for each band. From Fig. 8b, we can extract out that the lowest  $d_{xy}$  band has  $k_F = 0.28\pi/a_{\text{STO}}$ , while the next higher energy  $d_{xy}$  band has  $k_F = 0.21\pi/a_{\text{STO}}$  or  $2.3 \text{ nm}^{-1}$  and  $1.7 \text{ nm}^{-1}$ , respectively. Higher energy and less occupied bands have smaller  $k_F$ . These values, along with Eq. (6), allow us to convert the bound on  $\xi$  to a bound on  $l$ .

If  $l$  is approximately the same for all the interface bands, then  $\xi$  will be larger for the lower energy bands, which have the larger  $k_F$  and will progressively decrease for higher energy bands. This is the inverse of the trend needed for localization to hold. Thus, for localization to occur,  $l$  must be significantly larger for the higher energy bands. Namely, since the bands become more delocalized into the SrTiO<sub>3</sub> substrate with increasing energy, the interior of the SrTiO<sub>3</sub> substrate would have to be of high quality while the part with a few nm of the interface would have to be sufficiently disordered.

Following this logic and using the above numerical values in Eq. (6), we find the equivalent conditions that  $l < 3$  nm for the lowest band and  $l < 4$  nm for the higher  $d_{xy}$  bands. These values are small, considering the following standard estimation of mean free path:

$$l \sim \frac{\mu_H \hbar k_F}{e} \quad (7)$$

Taking a typical value of Hall mobility (see Table I)  $\mu_H \sim 10^3$  cm<sup>2</sup>V<sup>-1</sup>s<sup>-1</sup> and  $k_F \simeq 2$  nm<sup>-1</sup>, then we obtain  $l \sim 100$  nm. Regardless, assuming that a reasonable 2D cross section  $\sigma$  for a relevant defect is a few nanometers, the typical spacing of such defects in the interface plane is  $\sim \sqrt{l\sigma}$  and must also be on the order of a few nm or less.

We briefly consider what defects could produce such small  $l$ . One may dismiss surface steps or edge dislocations in the SrTiO<sub>3</sub> substrate. The former are typically hundreds of nm apart, and experiments indicate that they do not hinder transport, while the latter have a small areal density of  $\sim 10^{-8}$  nm<sup>-2</sup> [47]. The presence of extended defects every few nm can be excluded, as they would be visible in transmission electron microscopy (TEM) images of the interfaces. This means that point-like defects in the immediate vicinity of the interface are the most realistic possibility, and candidates include cation intermixtures and oxygen vacancies.

There is experimental evidence of La-Sr intermixture across the  $n$ -type interface [12, 38] on a scale of 1-2 nm. Son *et al.* [34] use this “interface roughness” as the basis for excluding states localized within  $\sim 2$  nm of the interface. However, this roughness is in the direction normal to the interface, whereas the relevant spacing is that of defects in the interface plane. For intermixtures to be responsible, La-Sr mixing must be rough over the scale of a few nm in the interface plane itself. Whether that occurs remains to be determined in future experiments and theoretical calculations.

Regarding oxygen vacancies, Nakagawa *et al.* [12] infer a small density of oxygen vacancies ( $0.10 \pm 0.04$  vacancies per 2D unit cell) at  $n$ -type interfaces. This defect density is of the right order of magnitude and might be considered a viable candidate for the disorder mechanism. Whether these oxygen vacancies have the necessary cross sections for scattering is a separate question. More importantly, oxygen vacancies at this density can in principle donate  $0.20e/a_{\text{STO}}^2$  ( $1.3 \times 10^{14}$  cm<sup>-2</sup>) to the interface, which is larger than the observed transport density. Even if the donation is imperfect, the number of electrons being added to the already electron-populated interface would be significant and these electrons would oc-

copy high energy, loosely bound states. They would greatly *increase* the number of electrons contributing to transport.

In summary, the Anderson localization scenario provides an attractive, yet still unsubstantiated, picture to explain the low sheet carrier densities observed in the transport experiments of Thiel *et al.* [47]. A more quantitative analysis of the situation leads us to the following conclusions: i) to induce the required localization, the mean free paths of states strongly bound to the interface must be smaller than those that are loosely bound; ii) the mean free path in the interface plane for the strongly bound states could be at most a few nm; and iii) point-like defects are likely scattering centers, with cation intermixtures or oxygen vacancies being possible candidates. While theoretically feasible, the localization scenario requires that a number of factors work hand in hand.

We end by noting that this localization scenario [30] is proposed to explain why theoretical values of sheet densities are higher than those found in the experiments of Thiel *et al.* [13]. On other hand, the sheet densities measured by Huijben *et al.* [55] are larger in magnitude, saturate to a value only a factor of two smaller than the theoretical value of  $0.5e/a_{\text{STO}}^2$ , and show a monotonic increase with  $\text{LaAlO}_3$  thickness, all in much closer agreement with existing theoretical findings.

#### 4. Spatial extent of the electron gas

As discussed in the review of experiments above, the experimental consensus for the thickness of the electron gas at the *n*-type interface is that it is confined to a length scale on the order of nanometers in the samples grown at high oxygen partial pressure ( $\sim 10^{-4}$  mbar) [16, 45, 57]. For samples grown at low oxygen partial pressure ( $\sim 10^{-6}$  mbar), the conduction electron gas extends hundreds of  $\mu\text{m}$  into the  $\text{SrTiO}_3$  substrate [41, 57]. In the latter case, the electrons may be due to extrinsic sources (*i.e.*, oxygen vacancies) and thus not determined by the intrinsic properties of the interface. The main contribution of *ab initio* theory in this matter is to provide detailed information about the shape and distribution of the electron gas in the intrinsic limit.

Janicka *et al.* [31] use double *n*-type symmetric supercells and find that the charge density profile of the electron gas follows an exponential decay,  $e^{-z/\delta}$  (where the first  $\text{TiO}_2$  layer is at  $z = 0$  and the  $\text{SrTiO}_3$  substrate is on the  $z > 0$  side). Fitting to DFT data, they obtain

$\delta \simeq 1$  nm. Due to the imposed symmetry, the geometry used by Janicka *et al.* [31] contains five SrTiO<sub>3</sub> unit cells of substrate ( $\sim 2$  nm). In our work [32], we use a stoichiometric *n*-type interface in a supercell with 11 u.c. of SrTiO<sub>3</sub>, and we find that the conduction electron density profile decays rapidly for the first few unit cells away from the interface, but has a longer, non-exponential tail further into the substrate. Son *et al.* [34] have performed the largest simulations to date with 15 to 30 u.c. of SrTiO<sub>3</sub> and also find exponential decay close to the interface that turns into an algebraic decay further into the substrate (see Fig. 5 of that work). Specifically, their calculations show that within 4 nm of the interface, the charge density decays exponentially with  $\delta = 1.84$  nm. Further into the SrTiO<sub>3</sub> substrate, the charge density profile is found to decay more slowly with the approximate form  $b/(z-z_0)$ .

### 5. Binding mechanism to the interface

The confinement of the electron gases at interfaces is usually attributed to band bending, a well-known concept in metal-oxide-semiconductor (MOS) interfaces. Janicka *et al.* [31] find that the confinement of the quasi 2D electron gas at the *n*-type interface of SrTiO<sub>3</sub>/LaAlO<sub>3</sub> is not solely due to band bending. They suggest that the formation of metal-induced-gap-states (MIGS) due to the presence of the conduction electrons at the interface plays an important role, allowing the electron gas to extend further into the SrTiO<sub>3</sub> substrate than simple band bending would allow.

An important question is why the electrons are bound to the interface in the first place. One answer is that, after the polar catastrophe takes place, the electrons at the *n*-type interface feel the electrostatic attraction from the holes on the other side of the LaAlO<sub>3</sub> film, and this attraction binds them to the interface. While this must play a role, it is not sufficient for the following two reasons. First, for the double *n*-type symmetric supercells, which have no polar fields and where there are no holes present to create the electrostatic attraction, DFT simulations still find a bound electron gas at the interface. This has already been reported in Refs. [30, 31]. In fact, for symmetric supercells with no polar fields, one would expect the electrons to occupy the lower-energy conduction band edge of the two materials (SrTiO<sub>3</sub> for this pair of materials) and to spread throughout the substrate. Second, holes at the *p*-type interface should feel the same attractive force, but instead are found to delocalize into the SrTiO<sub>3</sub> substrate. We report this effect for stoichiometric *p*-type interfaces [32] and

have verified that this holds for double  $p$ -type symmetric superlattices. Thus, the attraction of the opposite carriers across the  $\text{LaAlO}_3$  film is not sufficient to strongly bind them to the interface. Furthermore, there is an asymmetry between  $n$ -type and  $p$ -type interfaces in terms of binding carriers that is intrinsic to the interface structure itself.

We have proposed an explanation for this asymmetry [32]. In both  $\text{SrTiO}_3$  and  $\text{LaAlO}_3$ , the conduction band edge stems from the transition metal  $d$  orbitals. However, in  $\text{SrTiO}_3$  the Ti atoms are on the  $B$  site while in  $\text{LaAlO}_3$  the La atoms are on the  $A$  site (in the standard  $ABO_3$  notation). Thus in the bulk phase of  $\text{SrTiO}_3$ , the nearest Ti atoms are one lattice constant apart, but at the  $n$ -type  $\text{TiO}_2/\text{LaO}$  interface the Ti-La distance is  $\sqrt{3}/2$  times one lattice constant. This proximity, combined with the large spatial extent of the La  $d$  orbitals, enhances the tight-binding hopping element between the two transition metals to the extent that it becomes about 100 times larger than the hopping element between Ti  $d$  orbitals in bulk  $\text{SrTiO}_3$ . This large hopping matrix element creates a pair of bonding and antibonding states composed of superpositions of the Ti and La  $d$  states right at the interface: the low-energy bonding state is primarily of Ti  $d$  character and the anti-bonding one of La  $d$  character. Compared to the other Ti atoms in the  $\text{SrTiO}_3$  substrate, the Ti at the interface are special, as they have a lower energy and are thus the most favorable sites for electrons to accumulate when the metal-insulator transition takes place. (As detailed further below, the  $p$ -type interface has no enhanced hopping, and thus has no such special binding mechanism.)

In Ref. [32], we verify this explanation by mechanically moving the Ti at the interface to elongate (weaken) or shorten (strengthen) the Ti-La bond. As expected, when the Ti-La bond is strengthened, electrons more strongly localize towards the interface, and when the bond is weakened, electrons move farther into the substrate. As an alternate check, we compute the on-site energies of the transition metal  $d_{xy}$  orbitals from first principles in the interface region for a 4 u.c. thick  $\text{LaAlO}_3$  film that has undergone the polar catastrophe (within LDA). The results are shown in Fig. 9. The on-site energy for atom  $i$  is the diagonal matrix element  $\langle d_{xy}^i | \hat{H} | d_{xy}^i \rangle$ , where  $\hat{H}$  is the Kohn-Sham Hamiltonian and  $d_{xy}^i$  is the atomic orbital at that site. As expected, the La  $d_{xy}$  is at higher energy than the Ti  $d_{xy}$  due to the conduction band offset. The salient point of the figure is that the on-site energy of the Ti atom right at the interface is not the lowest one, but simulations show that the electron density is highest on the first interfacial Ti atom at the interface. The resolution to the

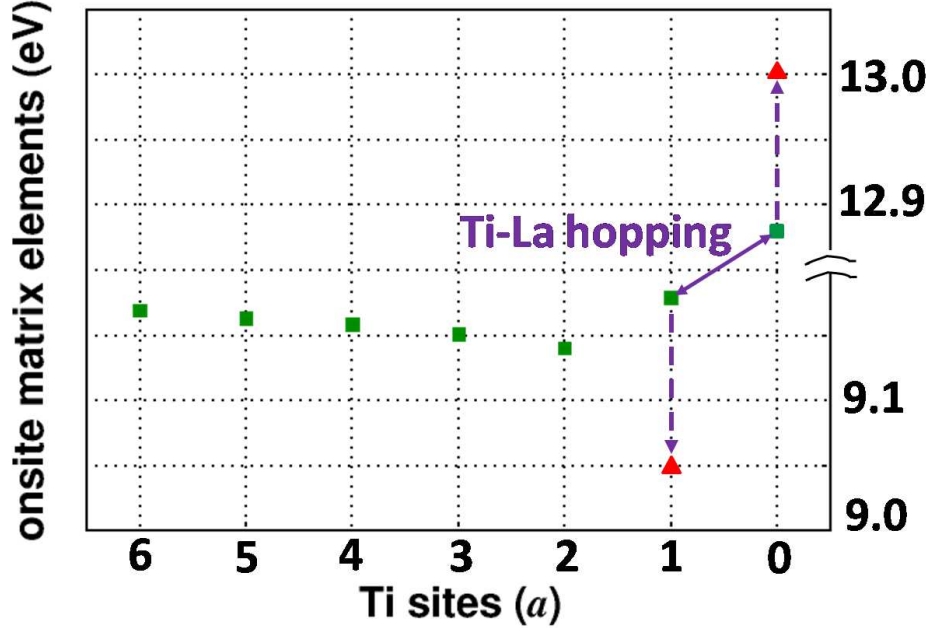


FIG. 9: Green squares show the on-site tight-binding matrix elements at the  $n$ -type interface computed from first principles for a simulation with 11 u.c. of  $\text{SrTiO}_3$  and 4 u.c. of  $\text{LaAlO}_3$  (the insulating-to-metallic transition occurs at this thickness in the DFT simulation). The on-site energies are for the Ti  $d_{xy}$  and La  $d_{xy}$  orbitals. The La atom is at site 0, and the Ti atoms are at sites 1-6. The  $n$ -type interface is located between sites 0 and 1. Note that the first Ti atom (at site 1) does not have the lowest on-site energy, but has the highest electron density. The red triangles show the effect of including the large hopping element between Ti and La at the interface. The La level is pushed up and the Ti level is pushed down, so inclusion of the hopping element now makes the first Ti the lowest energy site for electron accumulation.

puzzle is to include the large Ti-La hopping element of 0.7 eV. As indicated in Fig. 9, this pushes up the La level and lowers the Ti level at the interface. With this hopping included, the Ti at the interface is now the most favorable site for binding electrons and should accumulate the largest number of electrons.

These findings imply that the spatial extent of the electron gas is determined in large part by the Ti-La coupling at the interface. In particular, one does not expect to find an equally strongly bound electron gas when  $\text{LaAlO}_3$  is replaced by another perovskite in which the transition metal is either on the  $B$  site or has more localized atomic orbitals.

An experimental test of this prediction is straightforward in principle and requires epitaxial growth of other oxides on SrTiO<sub>3</sub> and the same types of measurements already performed for SrTiO<sub>3</sub>/LaAlO<sub>3</sub> interfaces. If this physical picture is correct, one can consider a number of possibilities for engineering the spatial profile and properties of the electron gas. Chemical substitutions right at the interface will change both the spatial extent of atomic orbitals as well as the interatomic spacings and thus modify the tight-binding hopping matrix elements. Alternately, mechanical motion of the transition metal atoms might be achieved by using piezoelectric or ferroelectric substrates that will in turn change the hopping elements through direct modifications of inter-atomic distances.

### 6. Magnetic ordering

As discussed above, experiments have shown intriguing magnetic properties at the SrTiO<sub>3</sub>/LaAlO<sub>3</sub> interface. Several groups have attempted to tackle the question of magnetic ordering at the interface theoretically with the LDA+U approach [24, 27, 29, 64].

Pentcheva and Pickett studied both unrelaxed [24] and relaxed [27]  $n$ -type interfaces using a  $c(2 \times 2)$  interface unit cell with  $U = 8$  eV and  $J = 1$  eV. They report that atomic relaxation does not play an important role in determining the magnetic states and their energetic orderings. The ground state in both cases is a ferromagnetic insulating state with disproportionated charge ordering in a checkerboard pattern in the plane of the interface. Perpendicular to the interface, they find that the excess 0.5 electrons per 2D cell are localized and reside in a single atomic plane right at the interface. Without the Hubbard  $U$  [27], they find that the ferromagnetic state and charge ordering are suppressed, that the interface is metallic, and that the excess electrons are delocalized over several SrTiO<sub>3</sub> unit cells.

Kelly *et al.* [29] use the rotationally invariant LDA+U method [71] with  $U = 5$  and  $J = 0.64$  eV. In contrast to the results of Pentcheva and Pickett, they find that the atomic geometry, in particular a GdFeO<sub>3</sub>-type distortion, is crucial in reducing the bandwidth of occupied Ti  $d$  states and in stabilizing magnetic orderings. Their ground state is a  $p(2 \times 2)$  anti-ferromagnetic insulating state with charge ordering. However, they point out that by imposing ferromagnetic ordering, they obtain a  $c(2 \times 2)$  insulating state with charge ordering, similar to the finding of Pentcheva and Pickett, which is 10 meV higher than their anti-ferromagnetic ground state. However, this energy difference is small, close to the limit

of their calculation accuracy [29].

Janicka *et al.* [64] use a  $(1 \times 1)$  interface unit cell and obtain different results. They find that when the excess electrons are forced to be confined to within 1.5 unit cells of SrTiO<sub>3</sub> at the interface, the ground state is a metallic ferromagnet, even in the absence of a Hubbard  $U$  correction. By increasing the SrTiO<sub>3</sub> thickness, they observe a decreasing magnetic moment and disappearance of the ferromagnetic state for 4.5 unit cells of SrTiO<sub>3</sub>. Upon applying  $U=5$  eV, they find that ferromagnetism is stabilized in the ground state for all the thicknesses (up to 4.5 SrTiO<sub>3</sub> unit cells). However, their interfaces remain metallic, in contrast to the above results. One explanation is that a  $(1 \times 1)$  unit cell is too small to allow for charge ordering — all Ti sites are forced to be equivalent, the eigenstates must be partially filled extended Bloch states, and one thus expects to find metallic behavior.

Charge ordering is an important ingredient in determining the correct magnetic ground state of the  $n$ -type interface, and the studies above demonstrate that accurate simulations require supercells with sufficient lateral extent to allow for this phenomenon. We end this section by noting that, while the LDA+ $U$  approaches to date have found magnetic states at the interface, the calculations with larger unit cells find insulating ground states, in contrast to experiments that report mobile electrons even at the lowest of temperatures.

### C. The $p$ -type interface

A number of first principles calculations have attempted to shed light on the insulating nature of the  $p$ -type interface as well as its general physical properties. For the insulating behavior, both intrinsic and extrinsic mechanisms have been investigated. Concomitant with the smaller number of experimental studies of this interface, there has also been less theoretical work on this system.

#### 1. Intrinsic $p$ -type interface: DFT results

Theoretical calculations that have used DFT within the standard LDA or GGA approach report a metallic state at the  $p$ -type interface [24, 25, 32]. The holes at the interface reside on the perovskite oxygen sublattice, their electronic states have essentially pure oxygen  $p$  character as expected for the valence band edge of a perovskite, and they occupy the top

portion of the valence band, creating a Fermi surface. At this level of description, the metallic character is clearly at odds with experiments.

As mentioned above, the holes at the  $p$ -type interface are not strongly bound to the interface but instead delocalize into the SrTiO<sub>3</sub> substrate. We have found this to hold for both stoichiometric  $p$ -type interfaces [32] as well as large double  $p$ -type symmetric supercells. Unlike the  $n$ -type interface, where binding is enhanced by the unusual Ti-La tight-binding hopping element, there appears to be no such binding force present for the  $p$ -type interface. The oxygen sublattice is continuous and unmodified across the  $p$ -type interface. Therefore, one does not expect any special hopping matrix element to be present, and calculations report that the oxygen-oxygen hopping elements are essentially constant and unchanged across the interface. The polar field in the LaAlO<sub>3</sub> will drive holes out of the LaAlO<sub>3</sub> film and into the SrTiO<sub>3</sub> film at the  $p$ -type interface, but once in the SrTiO<sub>3</sub>, the holes do not have any reason to be bound to the interface.

In our previous work [32], we investigate supercells with up to 11 u.c. of SrTiO<sub>3</sub>, and find that the holes are delocalized within the SrTiO<sub>3</sub> substrate for such thicknesses. The holes do feel the attractive electrostatic force from the electrons on the other side of the LaAlO<sub>3</sub> film. Therefore, one expects that the holes should be bound to the interface for thicker SrTiO<sub>3</sub> films. What the calculations show is that the length scale for the hole binding is larger than 11 SrTiO<sub>3</sub> unit cells, meaning that the binding energies will be weaker as well (when compared to the electrons at the  $n$ -type interface). At the DFT level, one expects an unbound or very weakly bound hole gas for the  $p$ -type interface. However, the DFT prediction of a metallic hole gas will still hold for such an ideal interface. For a more complete picture of how insulating behavior might arise in this picture, see the section III C 3 on oxygen vacancies further below.

## 2. *Intrinsic effects at the $p$ -type interface: the hole polaron*

Pentcheva and Pickett [24] investigate the possibility that strong correlation effects can induce a self-trapped hole polaron at the  $p$ -type interface. To this end, they use an LDA+U approach with  $U=7$  eV on the oxygen  $p$ -states. They study a symmetric double  $p$ -type superlattice with the atoms fixed in the ideal perovskite positions and a  $p(2\times 2)$  interface unit cell. They consider both ferromagnetic and anti-ferromagnetic orderings. The ferromagnetic

state they find exhibits disproportionated charge ordering and is half-metallic, at variance with the insulating behavior observed in experiments. They find the antiferromagnetic state to be charge ordered and insulating, with a very small energy gap of 50 meV. The half-metallic ferromagnetic state is energetically favored by 0.15 eV over the insulating antiferromagnetic state.

These results provide some evidence that correlation effects missing in LDA or GGA approaches can create interface electronic structures that differ from the simple metallic prediction of the LDA/GGA. With increasing  $U$ , charge-ordered localized states become energetically favored due to the increasing cost of double occupancy on an atomic site. Therefore, one expects a transition from the delocalized, metallic bands of the LDA/GGA prediction to localized states upon increasing  $U$ . Open questions are how sensitive these results are to the particular  $U$  value chosen and what the “correct” value of  $U$  may be. Separately, the above findings are based on unrelaxed atomic structures, and it is unclear whether atomic relaxation would favor antiferromagnetism.

### 3. Oxygen vacancies at the $p$ -type interface

Extrinsic effects such as those from defects or impurities may also help explain the insulating behavior of the  $p$ -type interface. Oxygen vacancies are one of the most prevalent defects in the SrTiO<sub>3</sub> substrate, and thus a number of research groups have focused on studying their interactions with the  $p$ -type interface. That oxygen vacancies can cause the insulating behavior was first suggested by Nakagawa *et al.* [12].

Pentcheva and Pickett [24] consider unrelaxed  $p$ -type superlattices with 25% of oxygen vacancies (*i.e.*, one oxygen vacancy per four 2D unit cells) in either the SrO or AlO<sub>2</sub> atomic planes at the SrO/AlO<sub>2</sub>  $p$ -type interface and find that the ground state is insulating and nonmagnetic in both cases. However, the Fermi level is found to be located in a narrow dip of the density of states, and the energy gap is too small to distinguish. (When examining oxygen vacancies, Pentcheva and Pickett do not apply the Hubbard  $U$  that they use when investigating the hole polaron.)

Park *et al.* [25] studied both unrelaxed and relaxed double  $p$ -type symmetric superlattices without Hubbard  $U$ . Upon allowing relaxation and including oxygen vacancies in the SrO plane at the interface, which favors oxygen vacancy formation over the AlO<sub>2</sub> layer, they find

that the  $p$ -type superlattice with 25% of oxygen vacancies remains metallic, in contrast to the prediction of the simple ionic limit. However, increasing the oxygen vacancy concentration to 50% results in insulating behavior. They suggest that strong hybridization between Ti  $d$ -orbitals and O  $p$ -orbitals close to the Fermi level makes it difficult for the two electrons of an oxygen vacancy to easily compensate the holes. This result is in qualitative agreement with the experimental finding that 32% oxygen vacancies per 2D unit cell (and not 25%) are found at the insulating  $p$ -type interface [12].

The above two studies employ symmetric superlattices and consider oxygen vacancies directly at the  $p$ -type interface. Our work on stoichiometric  $p$ -type supercells with a  $p(2 \times 2)$  interface unit cell [32] investigates the energetics of oxygen vacancy formation in the atomic planes at and away from the  $p$ -type interface. We find that, for a 25% oxygen vacancy concentration, the formation energy decreases as the oxygen vacancies move away from the  $p$ -type interface. The convergence to the bulk SrTiO<sub>3</sub> oxygen vacancy formation energy is achieved at a distance of three unit cells from the interface. These results show that the  $p$ -type interface repels oxygen vacancies, which instead prefer to stay in the bulk of the SrTiO<sub>3</sub> substrate.

Since both holes and vacancies are repelled by the interface, these results suggest that the interface region is not only defect free but also free of holes. Therefore, the interface itself will be insulating. The remaining issue is to understand why the holes do not contribute to transport. Based on the picture above, we propose the following qualitative possibility: the SrTiO<sub>3</sub> substrate will inevitably have some oxygen vacancies, either due to growth conditions or thermal fluctuations. As long as the SrTiO<sub>3</sub> substrate is thick enough to contain at least one oxygen vacancy per four 2D unit cell (a very low 3D concentration for a thick substrate), the holes can become trapped (*i.e.* annihilated) by the two electrons of the oxygen vacancy and thus will not contribute to transport. This hypothesis could be tested by large scale simulations that contain  $p$ -type interfaces, oxygen vacancies, and relatively thick SrTiO<sub>3</sub> slabs.

#### IV. OUTSTANDING PUZZLES

Despite experimental and theoretical efforts, the physical origins of some aspects of the SrTiO<sub>3</sub>/LaAlO<sub>3</sub> interface remain undetermined. We have mentioned several of these ques-

tions in the course of this progress report. In this section, we discuss them in more detail and suggest several experiments and computations that may help to further illuminate the underlying physics of the range of intriguing behavior observed in this remarkable system.

### A. Whence insulating *n*-type interfaces?

It is found in experiment that for samples grown at very high oxygen partial pressure ( $> 10^{-2}$  mbar) [40] or annealed at 300 mbar during cooling [41], the *n*-type interfaces can become completely insulating. In fact, the conducting properties of *n*-type interfaces become poorer with increasing  $p_{\text{O}_2}$  during the growth process (from  $10^{-6}$  to  $10^{-3}$  mbar) [41]. With presumably better stoichiometry control, one would expect that the transport properties would converge to those of an ideal interface, where the polar catastrophe plays the dominant role. What is noticeable is that the high-pressure growth experimental results are at variance with these expectations.

At first glance, this phenomenon would imply that the observed interface conductivity comes only from the oxygen vacancies. With the higher  $p_{\text{O}_2}$  or post-annealing to repair the oxygen off-stoichiometry, the concentration of oxygen vacancies should decrease, resulting in higher sheet resistance and lower sheet carrier density. However, the sheet carrier density does show an abrupt jump at 4 unit cells of  $\text{LaAlO}_3$  [13], which is difficult to explain using oxygen vacancy doping alone.

We mention here a number of possible scenarios and related questions. The first is that, for ideal *n*-type interfaces and for polar  $\text{LaAlO}_3$ , the polar catastrophe does not take place and that the theoretical models are unable to describe the correct physical properties. While logically possible, this scenario seems unlikely because the polar catastrophe for idealized interfaces is based on simple physical properties such as ionic charges of the cations. Next, one can consider the possibility that the theoretical results are correct but inapplicable; that the  $\text{LaAlO}_3$  becomes non-polar when the samples are grown under high  $p_{\text{O}_2}$  or post-annealed. Perhaps, aside from removing oxygen vacancies, the oxidation has other side effects. The oxidation introduces oxygen atoms at the surfaces of the samples which then diffuse into the body of the materials. Does a larger flux of oxygen through the lattice affect the cation sublattice by enhancing disorder and/or intermixing? Does one achieve sharp and ideal interfaces or is the disorder sufficient to make the  $\text{LaAlO}_3$  nonpolar?

Recent work by Segal *et al.* on molecular beam epitaxy grown SrTiO<sub>3</sub>/LaAlO<sub>3</sub> interfaces yield a number of interesting findings concerning some of these questions. Similar to Thiel *et al.* [13], a critical separation of 4 unit cells of LaAlO<sub>3</sub> is found, as well as similar sheet carrier densities in transport. However, x-ray spectra of the La core states do not reveal the expected LaAlO<sub>3</sub> polar field. Quantitatively, the polar field is  $\sim 10$  times smaller than the typical theoretical value of  $\sim 0.2$  eV/Å for samples with LaAlO<sub>3</sub> thicknesses below and above the critical separation. This provides some evidence that the LaAlO<sub>3</sub> may not be polar in some samples. However, it also creates puzzles: if the LaAlO<sub>3</sub> is not strongly polar, then what mechanism leads to a critical thickness close to the expected value?

One direct experimental probe for these questions is the electron energy loss spectroscopy (EELS) performed in the scanning transmission electron microscope (STEM). Detailed studies of the Ti, La, and O core level have provided valuable information on the distributions of the cations and oxygen vacancies at *n*-type and *p*-type interfaces [12]. However, we are not aware of data published to date on the La core levels for relatively thin LaAlO<sub>3</sub> films close to the critical thickness. The existence of the polar field in LaAlO<sub>3</sub> will lead to an energy shift between neighboring La core levels along the (001) LaAlO<sub>3</sub> film direction. An expected shift of about 0.7 eV per LaAlO<sub>3</sub> unit cell is within present experimental resolution. That will allow for direct visualization of the strength of the LaAlO<sub>3</sub> polar field.

On the theoretical front, because ideal interfaces and films may not provide a complete explanation, first principles studies can investigate aspects of disorder and intermixing. Specifically, which types of cation intermixtures are thermodynamically favored? What effect do they have on the polar field (if any)? Do they modify the critical separation or create new mechanisms for electron doping independent of the polar catastrophe? In addition, any experimental sample will have some degrees of off-stoichiometry. Theoretical studies of the possible importance of this disorder effect would be valuable.

## **B. What is the value of the critical separation?**

As discussed above, first principles simulations predict an *n*-type interface critical separation of 5 – 6 unit cells of LaAlO<sub>3</sub>. Recently, based on evidence from optical second harmonic generation, Savoia *et al.* [72] propose that, even at 3 unit cells of LaAlO<sub>3</sub>, electrons are injected into the interface but become localized. The conductance does not appear until the

electron gas becomes more uniform at a larger  $\text{LaAlO}_3$  thickness. Sing *et al.* [45] use hard x-ray photoelectron spectroscopy and find finite sheet carrier density at samples with 2 u.c. of  $\text{LaAlO}_3$ . They remark that part of the carrier concentration may be of intrinsic origin, but it does not lead to conduction.

What are some possible mechanisms that lead to a smaller critical separation than the polar catastrophe would predict? First, oxygen vacancies in the  $\text{SrTiO}_3$  substrate are an extrinsic doping mechanism that is unlikely here because it can not account simply for the abrupt insulating-to-metallic transition. Cation substitution [38] which results in the formation of metallic  $\text{La}_{1-x}\text{Sr}_x\text{TiO}_3$  is another possible mechanism. However, some details are not clear yet for this mechanism. What is the most stable distribution of cation substitution? How does cation substitution depend on the thickness of  $\text{LaAlO}_3$ ? In the very thin  $\text{LaAlO}_3$  films ( $< 4$  unit cells), is the cation mixing suppressed or enhanced? Cen *et al.* [21] have argued that the creation and annihilation of oxygen vacancies on the surface can induce an insulating-to-metallic transition, which raises some new important questions. How large is the formation energy of oxygen vacancies on the  $\text{LaAlO}_3$  surface? Does the formation energy depend on the thickness of  $\text{LaAlO}_3$ ? If thermodynamically favored, does kinetics allow the formation of oxygen vacancies on the surface on a reasonable time scale? There are likely other possible mechanisms that we have not mentioned here.

Overall, there appears to an incomplete agreement between experiment and theory concerning the value of the critical separation. This may suggest that the polar catastrophe at the ideal interface, while a reasonable starting point, does not capture all the physical effects at play, and that there can be other mechanisms that can generate metal-insulator transitions (*e.g.*, oxygen vacancies on the  $\text{LaAlO}_3$  surface).

### C. Is there conductivity on the surface?

Based on the polar catastrophe scenario, electrons transfer from the surface (or capping interface) to the  $n$ -type interface when the critical separation is exceeded. In principle, that should lead to two regions containing carriers and thus two conducting channels: electrons at the  $n$ -type interface and holes at the surface (or in the capping layers). However, to date, only electron-like carriers have been reported for the  $n$ -type interface. This is due in part to the fact that it is difficult for simple Hall measurements to detect multi-type carriers.

However, Thiel *et al.* [13] show in experiment that the conducting layer is not located on the  $\text{LaAlO}_3$  surface.

Although further experiments are needed to confirm the insulating behavior of the surfaces, Thiel's observation gives rise to the following question: if there are holes on the surface, why do they not contribute to the transport? One possible answer is self-trapping of the holes. The self-trapping can be similar in spirit to that of the self-trapped hole polaron proposed by Pentcheva and Pickett [24] at the  $p$ -type interface. Many details remain to be clarified. Does the presence of the surface enhance or destabilize self-trapping tendencies? What are the effects of surface relaxation? Are relatively large correlation effects (large Hubbard  $U_p$ ) still required for the polaron to form on the surface, and what is the correct Hubbard  $U_p$ ?

Cen *et al.* [21] propose that the presence of oxygen vacancies on the surface can dope the interface and make it conducting. In this picture, the electrons associated with the oxygen vacancies on the surface are pushed to the interface due to the  $\text{LaAlO}_3$  polar field. There are no holes on the surface, and the only conducting region is the interface which contains the electrons. This prediction is different from that of polar catastrophe mechanism, as the defects allow for a new degree of freedom. However, experimentally, it could be challenging to distinguish the following two cases: whether there are holes on the surface that do not conduct, or whether there are no holes at all. Further experiments may clarify the questions regarding holes on the  $\text{LaAlO}_3$  surface and could simultaneously give indications of what mechanisms come into play for thin  $\text{LaAlO}_3$  films.

#### **D. Are there multiple types of carriers?**

The possibility of multiple types of carriers being present at the  $n$ -type interface has been suggested in both the published experimental [19] and theoretical [30, 34] literature. Recent experiments also invoke the same picture [73]. Brinkman *et al.* [19] speculate that the magnetic phenomena they observe are due to spin scattering of itinerant electrons off of localized electrons that serve as localized magnetic moments. Seo *et al.* [73] explain their optical measurements based on the simultaneous presence of a low density of high-mobility carriers that dominate the transport properties at low temperatures, together with a high density of low-mobility carriers localized close to the interface that dominate the optical

spectra. The theoretical work uses the Anderson localization picture in 2D to argue that the bulk of the carriers, which are spatially localized close to the interface and highly 2D in nature, do not contribute to transport due to localization. The localization argument provides a possible explanation for why transport measurements on samples grown at higher  $p_{\text{O}_2} \sim 10^{-4}$  mbar show low sheet carrier densities when compared to the theoretical expectation of  $0.5e/a_{\text{STO}}^2$ .

The optical approach of Seo *et al.* [73] is exciting, as it has the potential to separate out different contributions from different types of carriers. To date, these experiments have been performed on samples grown at low  $p_{\text{O}_2} \sim 10^{-6}$  mbar, with correspondingly high sheet densities of up to  $3 \times 10^{17}$  cm<sup>-2</sup>, beyond the “intrinsic” limit of  $0.5e/a_{\text{STO}}^2$ . The majority of carriers may stem from oxygen vacancies, swamping out any signal from the intrinsic electron gas at the interface more evident in samples grown at higher  $p_{\text{O}_2}$ .

Regarding the Anderson localization scenario, one experiment is to try to grow similar samples but to find a way to modify the degree of disorder at the interface. That could be induced by intentionally introducing a low density of isovalent cations during growth of the interface region or by introducing intentional off-stoichiometry. More quantitatively speaking, from the estimation in Section III B 3, the required localization behavior requires mean free paths on the order of a few nanometers or less, which translates into point-like defects every nanometers as well. Since this spacing corresponds to only a few percent areal density per interface unit cell, the localization behavior should show strong dependence on the density of defects introduced on the percent level in the interface region. On the theoretical side, more detailed 2D transport modeling of the  $n$ -type interface, including scattering and thus localization, can help show whether the picture is applicable and under what conditions of disorder. In addition, the expected density and scattering efficacy of various defects (*e.g.*, oxygen vacancies or cation intermixtures) could be evaluated from first principles simulations.

## V. CONCLUSION

The SrTiO<sub>3</sub>/LaAlO<sub>3</sub> interface proves to be an excellent example which shows the richness of new phases emerging at complex oxide interfaces. The dependence of each new phase on the growth conditions and post-annealing procedures is not yet clear and warrants further

study, with a promising outlook towards various device applications of different functionalities. The SrTiO<sub>3</sub>/LaAlO<sub>3</sub> interface paves the way for engineering interfaces between transition metal oxides and serves as an archetype of polar-nonpolar interfaces. With advances in thin film growth techniques, many new heterointerfaces will emerge [74, 75], deepening our understanding of interface phenomena and extending the exceptional electronic properties in oxides.

### Acknowledgments

We acknowledge fruitful discussion or correspondence with Charles H. Ahn, Alexander Brinkman, Andrea Caviglia, Yoram Dagan, Alex Demkov, Victor E. Henrich, Paul J. Kelly, Jaekwang Lee, Jochen Mannhart, Richard M. Martin, Joe Ngai, Rossitza Pentcheva, Warren E. Pickett, James Reiner, Nicolas Reyren, Nicola Spaldin, Yaron Segal, Stefan Thiel, Jean-Marc Triscone, Evgeny Tsymbal, John C. Tully, Carlos A. F. Vaz and Frederick J. Walker. In particular, we are grateful to Charles H. Ahn, Victor E. Henrich and John C. Tully for their critical reading of our manuscript. This work is supported by the National Science Foundation under Contract No. MRSEC DMR 0520495. The Bulldog parallel clusters of the Yale High Performance Computing center provide computational resources.

- 
- [1] E. Dagotto, *Science* **318**, 1076 (2007).
  - [2] H. Y. Hwang, *Science* **313**, 1895 (2006).
  - [3] J. W. Reiner, F. J. Walker, and C. H. Ahn, *Science* **323**, 1018 (2009).
  - [4] M. Kawasaki, K. Takahashi, T. Maeda, R. Tsuchiya, M. Shinohara, O. Ishiyama, T. Yonezawa, M. Yoshimoto, and H. Koinuma, *Science* **266**, 1540 (1994).
  - [5] G. Koster, B. L. Kropman, G. J. H. M. Rijnders, D. H. A. Blank, and H. Rogalla, *Appl. Phys. Lett.* **73**, 2920 (1998).
  - [6] A. Ohtomo, D. A. Muller, J. L. Grazul, and H. Y. Hwang, *Nature* **427**, 423 (2004).
  - [7] A. Ohtomo and H. Y. Hwang, *Nature* **427**, 423 (2004).
  - [8] Y. Hotta, T. Susaki, and H. Y. Hwang, *Phys. Rev. Lett.* **99**, 236805 (2007).
  - [9] A. Kalabukhov, R. Gunnarsson, T. Claeson, and D. Winkler, *arXiv.org:0704.1050* (2007).

- [10] E. Bousquet, M. Dawber, N. Stucki, C. Lichtensteiger, P. Hermet, S. Gariglio, J.-M. Triscone, and P. Ghosez, *Nature* **452**, 732 (2007).
- [11] M. Takizawa, Y. Hotta, T. Susaki, Y. Ishida, H. Wadati, Y. Takata, K. Horiba, M. Matsunami, S. Shin, M. Yabashi, et al., *Phys. Rev. Lett.* **102**, 236401 (2009).
- [12] N. Nakagawa, H. Y. Hwang, and D. A. Muller, *Nature Mater.* **5**, 204 (2006).
- [13] S. Thiel, G. Hammerl, A. Schmehl, C. W. Schneider, and J. Mannhart, *Science* **313**, 1942 (2006).
- [14] C. Bell, S. Harashima, Y. Hikita, and H. Y. Hwang, *Appl. Phys. Lett.* **94**, 222111 (2009).
- [15] A. D. Caviglia, S. Gariglio, N. Reyren, D. Jaccard, T. Schneider, M. Gabay, S. Thiel, G. Hammerl, J. Mannhart, and J. M. Triscone, *Nature* **456**, 624 (2008).
- [16] N. Reyren, S. Thiel, A. D. Caviglia, L. F. Kourkoutis, G. Hammerl, C. Riether, C. W. Schneider, T. Kopp, A. S. Rüetschi, D. Jaccard, et al., *Science* **317**, 1196 (2007).
- [17] N. Reyren, S. Gariglio, A. D. Caviglia, D. Jaccard, T. Schneider, and J.-M. Triscone, *Appl. Phys. Lett.* **94**, 112506 (2009).
- [18] T. Schneider, A. D. Caviglia, S. Gariglio, N. Reyren, and J.-M. Triscone, *Phys. Rev. B* **79**, 184502 (2009).
- [19] A. Brinkman, M. Huijben, M. V. Zalk, J. Huijben, U. Zeitler, J. C. Maan, W. G. V. der Wiel, G. Rijnders, D. H. A. Blank, and H. Hilgenkamp, *Nature Mater.* **6**, 493 (2007).
- [20] C. Cen, S. Thiel, J. Mannhart, and J. Levy, *Science* **323**, 1026 (2009).
- [21] C. Cen, S. Thiel, G. Hammerl, C. W. Schneider, K. E. Andersen, C. S. Hellberg, J. Mannhart, and J. Levy, *Nature Mater.* **7**, 298 (2008).
- [22] G. Rijnders and D. H. A. Blank, *Nature Mater.* **7**, 270 (2008).
- [23] S. Gemming and G. Seifert, *Acta Mater.* **54**, 4299 (2006).
- [24] R. Pentcheva and W. E. Pickett, *Phys. Rev. B* **74**, 035112 (2006).
- [25] M. S. Park, S. H. Rhim, and A. J. Freeman, *Phys. Rev. B* **74**, 205416 (2006).
- [26] J. M. Albina, M. Mrovec, B. Meyer, and C. Elsässer, *Phys. Rev. B* **76**, 165103 (2007).
- [27] R. Pentcheva and W. E. Pickett, *Phys. Rev. B* **78**, 205106 (2008).
- [28] J. Lee and A. A. Demkov, *Phys. Rev. B* **78**, 193104 (2008).
- [29] Z. Zhong and P. J. Kelly, *Europhys. Lett.* **84**, 27001 (2008).
- [30] Z. S. Popović, S. Satpathy, and R. M. Martin, *Phys. Rev. Lett.* **101**, 256801 (2008).
- [31] K. Janicka, J. P. Velev, and E. Y. Tsybal, *Phys. Rev. Lett.* **102**, 106803 (2009).

- [32] H. Chen, A. M. Kolpak, and S. Ismail-Beigi, Phys. Rev. B **79**, 161402 (2009).
- [33] R. Pentcheva and W. E. Pickett, Phys. Rev. Lett **102**, 107602 (2009).
- [34] W. joon Son, E. Cho, B. Lee, J. Lee, and S. Han, Phys. Rev. B **79**, 245411 (2009).
- [35] U. Schwingenschlögl and C. Schuster, Europhys. Lett. **81**, 17007 (2008).
- [36] U. Schwingenschlögl and C. Schuster, Europhys. Lett. **86**, 27005 (2009).
- [37] U. Schwingenschlögl and C. Schuster, Chem. Phys. Lett. **467**, 354 (2009).
- [38] P. R. Willmott, S. A. Pauli, R. Herger, C. M. Schlepütz, D. Martocchia, B. D. Patterson, B. Delley, R. Clarke, D. Kumah, C. Cionca, et al., Phys. Rev. Lett. **99**, 155502 (2007).
- [39] V. Vonk, M. Huijben, K. J. I. Driessen, P. Tinnemans, A. Brinkman, S. Harkema, and H. Graafsma, Phys. Rev. B **75**, 235417 (2007).
- [40] A. Kalabukhov, R. Gunnarsson, J. Börjesson, E. Olsson, T. Claeson, and D. Winkler, Phys. Rev. B **75**, 121404(R) (2007).
- [41] G. Herranz, M. BasletiĆ, M. Bibes, C. CarrÉtero, E. Tafra, E. Jacquet, K. Bouzouane, C. Deranlot, A. HamziĆ, J. M. Broto, et al., Phys. Rev. Lett. **98**, 216803 (2007).
- [42] W. Siemons, G. Koster, H. Yamamoto, W. A. Harrison, G. Lucovsky, T. H. Geballe, D. H. A. Blank, and M. R. Beasley, Phys. Rev. Lett. **98**, 196802 (2007).
- [43] K. Yoshimatsu, R. Yasuhara, H. Kumigashira, and M. Oshima, Phys. Rev. Lett. **101**, 026802 (2008).
- [44] J.-L. Maurice, G. Herranz, C. Colliex, I. Devos, C. CarrÉtero, A. BarthÉlÉmy, K. Bouzouane, S. Fusil, D. Imhoff, E. Jacquet, et al., Europhys. Lett. **82**, 17003 (2008).
- [45] M. Sing, G. Berner, A. M. K. Goß, A. Ruff, A. Wetscherek, S. Thiel, J. Mannhart, S. A. Pauli, C. W. Schneider, P. R. Willmott, et al., Phys. Rev. Lett. **102**, 176805 (2009).
- [46] M. Salluzzo, J. C. Cezar, N. B. Brookes, V. Bisogni, G. M. D. Luca, C. Richter, S. Thiel, J. Mannhart, M. Huijben, A. Brinkman, et al., Phys. Rev. Lett. **102**, 166804 (2009).
- [47] S. Thiel, C. W. Schneider, L. F. Kourkoutis, D. A. Muller, N. Reyren, A. D. Caviglia, S. Gariglio, J.-M. Triscone, and J. Mannhart, Phys. Rev. Lett. **102**, 046809 (2009).
- [48] J. N. Eckstein, Nature Mater. **6**, 473 (2007).
- [49] G. A. Baraff, J. A. Appelbaum, and D. R. Hamann, Phys. Rev. Lett. **38**, 237 (1977).
- [50] W. A. Harrison, E. A. Kraut, J. R. Waldrop, and R. W. Grant, Phys. Rev. B **18**, 4402 (1978).
- [51] Y. Fujishima, Y. Tokura, T. Arima, and S. Uchida, Phys. Rev. B **46**, 11167 (1992).
- [52] T. Higuchi, D. Baba, T. Takeuchi, T. Tsukamoto, Y. Taguchi, Y. Tokura, A. Chainani, and

- S. Shin, *Phys. Rev. B* **68**, 104420 (2003).
- [53] M. Huijben, A. Brinkman, G. Koster, G. Rijnders, H. Hilgenkamp, and D. H. A. Blank, *Adv. Mat.* **21**, 1665 (2009).
- [54] J. Mannhart, D. H. A. Blank, H. Y. Hwang, A. J. Millis, and J. M. Triscone, *MRS Bull.* **33**, 1027 (2008).
- [55] M. Huijben, G. Rijnders, D. H. A. Blank, S. Bals, S. V. Aert, J. Verbeeck, G. V. Tendeloo, A. Brinkman, and H. Hilgenkamp, *Nature Mater.* **5**, 556 (2006).
- [56] F. J. Wong, M. Chi, R. V. Chopdekar, B. B. Nelson-Cheeseman, N. D. Browning, and Y. Suzuki, [arXiv.org:0809.0926](https://arxiv.org/abs/0809.0926) (2008).
- [57] M. Basletic, J.-L. Mauric, C. Carrétéro, G. Herranz, O. Copie, M. Bibes, E. Jacquet, K. Bouzouane, S. Fusil, and A. Barthélémy, *Nature Mater.* **7**, 621 (2008).
- [58] M. van Zalk, J. Huijben, A. J. M. Giesbers, M. Huijben, U. Zeitler, J. C. Maan, W. G. van der Wiel, G. Rijnders, D. H. A. Blank, H. Hilgenkamp, et al., [arXiv.org:0806.4450](https://arxiv.org/abs/0806.4450) (2008).
- [59] M. B. Shalom, C. W. Tai, Y. Lereah, M. Sachs, E. Levy, D. Rakhmilevitch, A. Palevski, and Y. Dagan, *Phys. Rev. B* **80**, 140403 (2009).
- [60] W.-C. Lee and A. H. MacDonald, *Phys. Rev. B* **76**, 075339 (2007).
- [61] W. Kohn and L. J. Sham, *Phys. Rev.* **140**, A1133 (1965).
- [62] J. P. Perdew, K. Burke, and M. Ernzerhof, *Phys. Rev. Lett.* **77**, 3865 (1996).
- [63] V. I. Anisimov, F. Aryasetiawan, and A. I. Lichtenstein, *J. Phys.: Condens. Matter* **9**, 767 (1997).
- [64] K. Janicka, J. P. Velev, and E. Y. Tsympal, *J. Appl. Phys.* **103**, 07B508 (2008).
- [65] N. C. Bristowe, E. Artacho, and P. B. Littlewood, *Phys. Rev. B* **80**, 045425 (2009).
- [66] A. F. Devonshire, *Philos. Mag.* **40**, 1040 (1949).
- [67] A. Antons, J. B. Neaton, K. M. Rabe, and D. Vanderbilt, *Phys. Rev. B* **71**, 024102 (2005).
- [68] I. Souza, J. Íñiguez, and D. Vanderbilt, *Phys. Rev. Lett.* **89**, 117602 (2002).
- [69] P. A. Lee and T. V. Ramakrishnan, *Rev. Mod. Phys.* **57**, 287 (1985).
- [70] E. P. Abrahams, P. W. Anderson, D. C. Licciardello, and T. V. Ramakrishnan, *Phys. Rev. Lett.* **42**, 673 (1979).
- [71] A. I. Liechtenstein, V. I. Anisimov, and J. Zaanen, *Phys. Rev. B* **52**, R5467 (1995).
- [72] A. Savoia, D. Paparo, P. Perna, Z. Ristic, M. Salluzzo, F. M. Granozio, U. S. di Uccio, C. Richter, S. Thiel, J. Mannhart, et al., *Phys. Rev. B* **80**, 075110 (2009).

- [73] S. S. A. Seo, Z. Marton, W. S. Choi, G. W. J. Hassink, D. H. A. Blank, H. Y. Hwang, T. W. Noh, T. Egami, and H. N. Lee, *Appl. Phys. Lett.* **95**, 082107 (2009).
- [74] M. K. Niranjana, Y. Wang, S. S. Jaswal, and E. Y. Tsymbal, *Phys. Rev. Lett.* **103**, 016804 (2009).
- [75] Y. Wang, M. K. Niranjana, J. D. Burton, J. M. An, K. D. Belashchenko, and E. Y. Tsymbal, *Phys. Rev. B* **79**, 212408 (2009).